Alma Mater Studiorum · Università di Bologna

Scuola di Ingegneria e Architettura · Sede di Cesena
Corso di Laurea Magistrale in
elettronica e telecomunicazioni per l'energia

CHANNEL ESTIMATION SCHEMES IN THE PRESENCE OF RECONFIGURABLE INTELLIGENT SURFACES

Tesi di Laurea Magistrale in
Sistemi di Telecomunicazioni LM

Relatore:
Chiar.mo Prof. Ing.
DAVIDE DARDARI

Correlatrice:
Dott. Ing.
ANNA GUERRA

Presentata da:
GIACOMO GIORGINI

III sessione
Anno Accademico 2019/2020

Acronyms

SNR Signal-to-Noise Ratio

UDN Ultra-Dense Network

MIMO Multiple-Input Multiple-Output

RF Radio Frequency

LNA Low Noise Amplifier

ADC Analog-to-Digital Converter

SRE Smart Radio Environment

RIS Reconfigurable Intelligent Surface

FPGA Field-Programmable Gate Array

PIN Positive-Intrinsic-Negative

FET Field-Effect Transistor

MEMS Micro-Electromechanical System

CSI Channel State Information

SISO Single-Input Single-Output

MSE Mean Square Error

EM Electromagnetic field

LOS Line-Of-Sight

ML Maximum Likelihood

CDF Cumulative Density Function

Sommario

Il progetto di tesi svolto riguarda lo studio di alcuni schemi di stima del canale di propagazione in presenza di superfici intelligenti riconfigurabili (comunemente chiamate RIS, reconfigurable intelligent surfaces).
In particolare, nel Capitolo 1, viene prima di tutto descritto lo scenario in cui avere a disposizione una RIS che guidi opportunamente il segnale trasmesso può essere vantaggioso (se non necessario nei futuri sistemi cellulari), per poi analizzare, nel Capitolo 2, in maniera più dettagliata cosa sia una RIS, come può essere modellata, e come cambia il protocollo di comunicazione in presenza di tali superfici, evidenziando l'importanza e la difficoltà di trovare delle tecniche di stima del canale in scenari di questo genere.
Nel Capitolo 3 viene presentato lo stato dell'arte relativo ai principali approcci di stima del canale studiati in letteratura, facendo anche una suddivisione delle varie casistiche. Sempre nello stesso capitolo, viene analizzato nel dettaglio uno dei principali approcci ottimi validi nel caso di sistemi singola antenna (single-input single-output - SISO), in cui la comunicazione viene assistita da una singola RIS, ed un secondo approccio valido nel caso di sistemi multi-antenna (multiple-input multiple-output -MIMO).
Essendo evidente come il principale problema riguardante la maggior parte degli approcci studiati in letteratura (sia ottimi che sub-ottimi) sia il numero elevato di toni pilota necessari nella fase di training per stimare il canale, nel Capitolo 4 viene proposto un nuovo algoritmo, valido nel caso SISO, in grado di superare questo grosso limite. In particolare, viene analizzato come si presenta il profilo di fase del canale sia in condizioni di campo lontano che campo vicino, e viene poi illustrato nel dettaglio come tali informazioni possono essere sfruttare per stimare il canale tramite un approccio maximum likelihood. Le simulazioni che seguono, fanno vedere come un simile approccio sia in grado di ottenere delle valide stime delle informazioni di canale sfruttando solamente il 10/15% dei toni pilota necessari nell'approccio ottimo descritto nel Capitolo 3. Sempre nello stesso capitolo, viene evidenziato come il problema di stima del canale sia equivalente al problema di stima della posizione del ricevitore. In particolare, note le posizioni del trasmetti-

tore e della RIS adottata, viene illustrato un metodo (strettamente collegato all'approccio di stima del canale) di stima della posizione del ricevitore. Infine, nel Capitolo 5, vengono presentate le conclusioni e possibili sviluppi futuri correlati all'algoritmo proposto nel capitolo precedente.

Summary

The thesis activity developed is about the study of some propagation channel estimation schemes in the presence of reconfigurable intelligent surfaces (commonly called RISs).
In particular, in Chapter 1, it is described the scenario in which having a RIS available to guide appropriately the transmitted signal can be advantageous (if not necessary in future cellular systems), whereas, in Chapter 2, how a RIS works is analyzed in more detail by describing the typical models and how the communication protocol changes in the presence of such surfaces, highlighting the importance and difficulty of finding channel estimation techniques in RIS-assisted wireless network.
Chapter 3 presents the state of the art relating to the main channel estimation approaches studied in the literature, also making a classification of the various case studies. In the same chapter, one of the main optimal approaches valid in the singe-input single-output (SISO) case, in which the communication is assisted by a single RIS, is analyzed in detail and then a second valid approach for the multiple-input multiple-output (MIMO) scenario is presented.
Being evident that the main problem concerning most of the approaches studied in the literature (both optimal and sub-optimal) is about the high number of pilot tones required in the training phase to estimate the channel, in Chapter 4 a novel algorithm is proposed, valid in the SISO case, able to overcome this big limit. In particular, it is analyzed the phase profile of the channel both in far-field and near-field channel conditions, and then it is illustrated in detail how this information can be exploited to estimate the channel through a maximum likelihood approach. The simulations that follow show how this approach is able to obtain valid estimates of the channel information by exploiting only the 10/15% of the pilot tones needed in the optimal approach described in Chapter 3. In the same chapter, it is highlighted how the channel estimation problem is equivalent to the receiver position estimation problem. In particular, once the positions of the transmitter and the RIS adopted are known, a method (strictly connected to the channel estimation

approach) for estimating the position of the receiver is illustrated. Finally, in Chapter 5, the conclusions and possible future developments related to the algorithm proposed in the previous chapter are discussed.

Contents

Chapter 1

Smart Radio Environments

1.1 Digital communication in noisy channels

The goal of a wireless communication system is to create a network where all the nodes belonging to the network itself can exchange the greatest amount of information with the highest reliability. The challenge of preserving a high reliability arises from the fact that any propagation channel is noisy: the noise represents a source of disturbance for communications, leading to a trade off between the quantity of information sent per unit of time and the reliability of the information itself.
In a digital communication system, the information is described in the form of discrete symbols: we talk about symbol rate, that is the number of information (symbols) per unit of time. The symbol rate depends on the bit rate and on the specific modulation technique adopted.
Given a communication system, a well-known figure of merit for the reliability of information is represented by the error probability, that it is seen as the probability to receive a different symbol (or message) with respect to the transmitted one; it is a decreasing function of the signal-to-noise ratio (SNR) defined as follow:

$$\mathrm{SNR} = \frac{\mathrm{S}}{\mathrm{N}} = \frac{\mathrm{E_b} \cdot \mathrm{B_r}}{\mathrm{N_0} \cdot \mathrm{B}}$$

where $\mathrm{B_r}$ represents the bit rate, B the bandwidth of the modulated signal and $\mathrm{N_0} \cdot \mathrm{B}$ the noise power (being $\mathrm{N_0}$ the one-sided noise spectral density). In the hypothesis of fixed transmission power S, it can be noted that an increasing of the bit rate leads to a lower energy per bit with a consequent decreasing of SNR (because of B is proportional to $\mathrm{B_r}$) and a decreasing of performance.

Given a propagation channel, it is known from the Shannon-Hartley theorem the expression of channel capacity C:

$$C = B(1 + \log_2 SNR)$$

As it can be seen, the capacity is a function of the SNR and of the bandwidth B. Always from Shannon theorem, the channel capacity represents also the maximum bit rate that permits to obtain any desired low level of error probability. We can note that the increasing of B is more advantageous rather than an increasing of SNR, because of the logarithm.
Applications that require an ever increasing number of highly reliable information per unit of time pushed to the use of higher and higher frequencies, exploiting and discovering new portions of the power spectrum, according to the use of higher carrier frequency with a wider bandwidth B.

1.2 Towards 6G: TeraHertz communications

Looking at the evolution of cellular systems through different generations, the common denominator is:

- Higher bit rate;
- Lower latency;
- Possibility of managing more and more users.

In particular, in 5G system, the bit rate is set equal to 20 Gb/sec, the maximum latency is 10 ms and there is the possibility of managing a massive number of IoT nodes. The targeted 1000-fold network capacity increase and ubiquitous wireless connectivity for at least 100 billion devices by the forthcoming fifth-generation wireless network could be achieved thanks to the various key enabling technologies such as:

- Ultra-dense network (UDN);
- Massive multiple-input multiple-output (MIMO);
- Millimeter wave (mmWave) communication.

However, according to [1], the required high complexity and hardware cost as well as the increased energy consumption are still crucial issues that remain unsolved. For instance, densely deploying base stations or access points in

a UDN not only entails an increased hardware deployment and maintenance cost, but also aggravates the network interference issue. In addition, extending massive MIMO from sub-6 GHz to mmWave frequency bands generally requires more complex signal processing as well as more costly and energy consuming hardware (e.g., radio frequency (RF) chains). Therefore, current research has focused on finding effective solutions for energy and spectral efficient beyond 5G wireless cellular network.
We can summarize the goals and characteristics of the 5G system by comparing the futures beyond-5G and 6G systems in the following table:

	5G	Beyond 5G	6G
Application types	• eMBB •URLLC •mMTC	• Reliable eMBB •URLLC •mMTC •Hybrid (URLLC + eMBB)	New applications: • MBRLLC • mURLLC • HCS • MPS
Device types	• Smartphones • Sensors • Drones	• Smartphones • Sensors • Drones •XR equipment	• Sensors and DLT devices • CRAS • XR and BCI equipment • Smart implants.
Spectral and energy efficiency gains[1] with respect to today's networks	10x in bps/Hz/m^2/Joules	100x in bps/Hz/m^2/Joules	1000x in bps/Hz/m^3/Joules (volumetric)
Rate requirements	1 Gb/s	100 Gb/s	1 Tb/s
End-to-end delay requirements	5 ms	1 ms	< 1 ms
Radio-only delay requirements	100 ns	100 ns	10 ns
Processing delay	100 ns	50 ns	10 ns
End-to-end reliability requirements	99.999 percent	99.9999 percent	99.99999 percent
Frequency bands	• Sub-6 GHz • MmWave for fixed acces.	• Sub-6 GHz • MmWave for fixed access	• Sub-6 GHz • MmWave for mobile acces • Exploration of higher frequency and THz bands (above 300 GHz) • Non-RF (e.g., optical, VLC, etc.)
Architecture	• Dense sub-6 GHz small base stations with umbrella macro base stations. • MmWave small cells of about 100 m (for fixed access).	• Denser sub-6 GHz small cells with umbrella macro base stations • < 100 m tiny and dense mmWave cells	• Cell-free smart surfaces at high frequency supported by mmWave tiny cells for mobile and fixed access. • Temporary hotspots served by drone-carried base stations or tethered balloons • Trials of tiny THz cells.

[1] Here, spectral and energy efficiency gains are captured by the concept of area spectral and energy efficiency.

Figure 1.1: Requirements of 5G *vs* Beyond-5G *vs* 6G [2].

To satisfy 6G requirements shown in figure 1.1, a leap in the frequency band is necessary and THz communications seem a promising solution.
Despite the fact that by definition the THz band extends from 300 GHz to 10 THz, researchers have found it convenient to categorize beyond 100 GHz applications as THz communications (today referred to also as a sub-THz band), below such a threshold the millimeter-wave bands of 5G are defined. Unlike mmWave communications, THz communications can achieve a terabit/second data rate without any spectral efficiency enhancement tech-

nique such as MIMO. Furthermore, according to [3], due to their shorter wavelengths, THz communication systems present the following advantages:

- They can support higher link directionality;
- They are less susceptible to free-space diffraction;
- They are less susceptible to inter-antenna interference;
- They can be realized in much smaller footprints;
- They possess higher resilience to eavesdropping.

On the other hand, it is important to focus on the problems that arise when higher frequencies are adopted. Hereafter, we can recall the most important ones [3]:

- Higher propagation path loss;
- Higher obstruction from obstacles;
- Larger insertion losses in the RF frontend;
- More low noise amplifier (LNA);
- More analog-to-digital converter (ADC) noise;
- Lower power amplifier efficiency compared to lower frequencies.

In conclusion, high frequencies offer the benefit of large channel bandwidths and, thus, high throughput, low latency and high capacity: in particular, THz band communications are expected to play a pivotal role in the upcoming 6G of wireless mobile communications, enabling ultra-high bandwidth and ultra-low latency communication paradigms. On the other hand, many challenges need to be addressed before the widespread use of THz communications. For instance, high propagation losses and power limitations result in very short communication distances, and frequency-dependent molecular absorptions result in band-splitting and bandwidth reduction. The improvements that can be expected by operating only on the end-points of the wireless environment may not be sufficient to fulfill the challenging requirements of future wireless network.

1.3 Definition of a smart radio environment

Due to the very high frequencies exploited in future wireless networks, path loss attenuation becomes the main problem to manage in order to guarantee an adequate SNR to the receiver. A typical mobile network base station transmits radio waves in the order of magnitude of Watts while a user equipment receives signals of the order of magnitude of microWatts when operating at high frequencies [4]. Hence, researchers are putting efforts in understanding how to not waste such a huge amount of power in the environment, for example, by recovering it using new materials and techniques. A possibility is to re-think the wireless environment as an active entity able to reshape and guide the propagation, and not as a passive reflector. In this direction, reflecting materials, for example metamaterials, can be used to coat walls in order to focus the multipath towards the desired destinations and, hence, to avoid a dispersion of useful contributions.

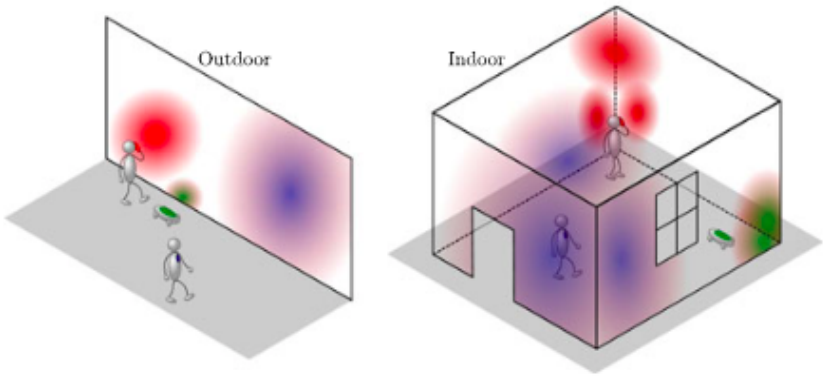

Figure 1.2: Three users communicating with intelligent surfaces, in an outdoor and an indoor scenario, respectively [5].

As depicted in figure 1.2, the key idea is to imagine a technology that permits to program in real-time the reflection angle of the walls, obtaining an "intelligent" environment that can always favor the propagation, whatever are the positions of the transmitter and the receiver.
In this way, according to [4], the propagation channel itself becomes an optimization variable of the system in addition to the transmitter and the receiver. This approach is referred to as a Smart Radio Environment (SRE) or Wireless 2.0 in order to emphasize the conceptual and fundamental difference with the design and optimization criteria adopted in current and past

generations of wireless network, as shown in figure 1.3.

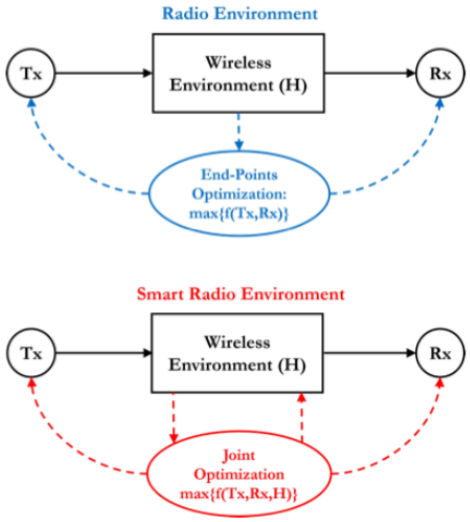

Figure 1.3: Radio environments *vs* smart radio environments [4].

In contrast to current wireless networks where the environment is out of control of the telecommunication operators, a smart radio environment is a wireless network where the environment is turned into a smart reconfigurable space that plays an active role in transferring and processing information. Wireless networks, in particular, are rapidly evolving towards a software-based and reconfigurable platform, where every part of the network will be capable of adapting itself to the changes of the environment. Broadly speaking, according to [6], current wireless networks operate according to three main postulates:

1) The environment is usually perceived as an "unintentional adversary" to communication and information processing;

2) Only the end-points of the communication network are usually optimized;

3) Wireless network operators have usually no control of the environment.

Apart from being uncontrollable, the environment has usually a negative effect on the communication efficiency and the quality of service: the signal attenuation limits the radio connectivity, multipath propagation results in fading phenomena, and reflections and refractions from large objects are the main sources of uncontrollable interference. In smart radio environments,

on the other hand, as depicted in figure 1.4, the wireless environment itself is turned into a software-reconfigurable entity, whose operation is optimized to enable uninterrupted connectivity, high quality of service, and where the information is transmitted without necessarily generating new signals but recycling the existing ones whenever possible.

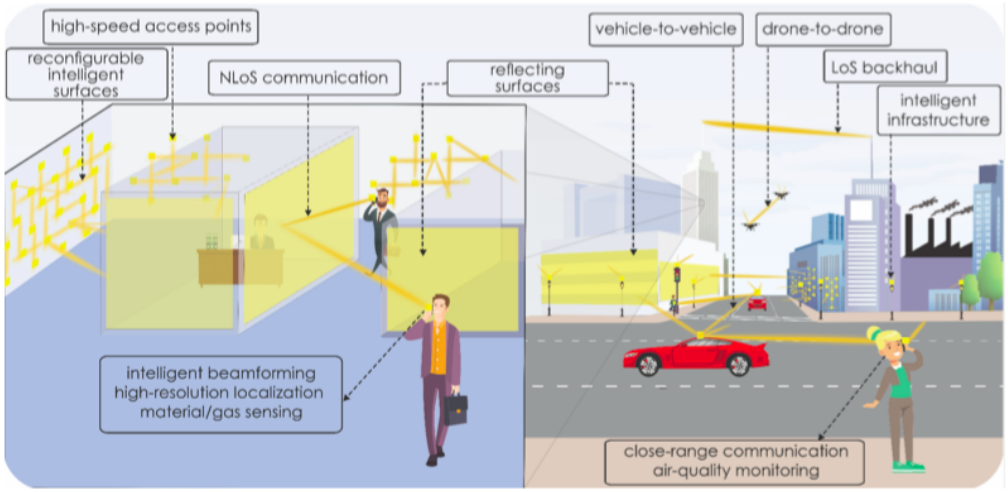

Figure 1.4: A vision of communications in a smart radio environment [3].

Conceptually, the difference between current wireless networks and smart radio environments is shown in figure 1.5.

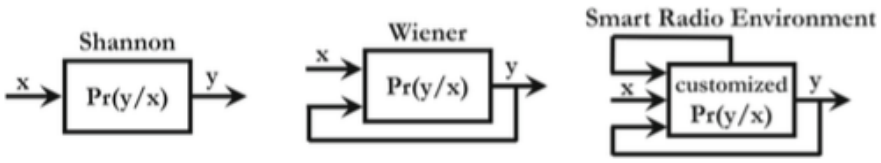

Figure 1.5: New communication-theoretic model for smart radio environments [6].

Recalling the previous figure, according to Shannon the system model is given and it is formulated in terms of transition probabilities (i.e., Pr(y / x), where x is the message send, y the received and Pr(y / x) represents the probability to obtain y given x). According to Wiener, the system model is still given, but its output is fed back to the input, which is optimized by taking the output into account (for example, the channel state is sent from a receiver back to a transmitter for channel-aware beamforming). In smart

radio environments, by contrast, the environment can be customized in order to obtain the desired system model.
The key enabler technology to realize the vision of SREs, by making the wireless environment programmable and controllable, is the so-called RIS (Reconfigurable Intelligent Surface).

Chapter 2

RIS: Reconfigurable Intelligent Surface

2.1 Description of a RIS

A RIS (or IRS) can be seen as a matrix of N smart reflective/radiating elements, that can be programmed by adjusting their phases through phase-shifters and, eventually, adjusting their amplitudes (by considering the attenuation of the impinging signal).

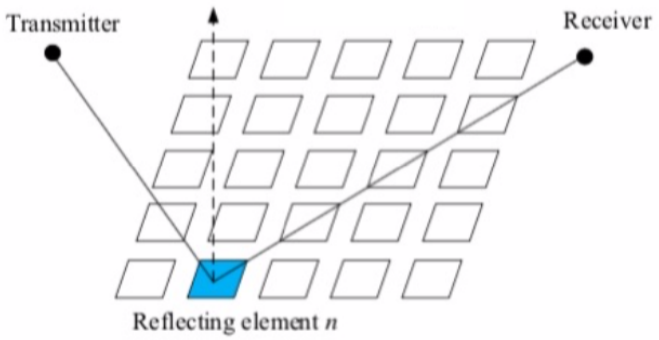

Figure 2.1: RIS as a surface with a discrete number of reflecting elements [7].

The RIS can be made with inexpensive adaptive (smart) thin composite material sheet, which, similar to a wallpaper, covers parts of walls, buildings, obstacles, etc., capable of modifying the radio waves impinging upon it in ways that can be programmed and controlled by using external stimuli. In this way, it can be possible to control the phase and the amplitude of the

signals impinging at each radiating element, so that the propagation can be guide in the desired manner. A prominent property of RISs is, therefore, the capability of being (re-)configurable after their deployment in a wireless environment.
Based on this general definition, the operation of a RIS can, in general, be split into two phases that are executed periodically based on the coherence time of the environment [4].

- ***Control and programming phase***: the necessary environmental information for configuring the operation of the RIS is estimated, and it is configured for subsequent operation.
- ***Communication phase***: the RIS is configured already and assists the transmission of other devices throughout the network.

There are different ways to conceive a RIS, but the main possible implementations are using reflectarray and metasurface [8].

1) Reflectarray-based RIS The simplest way to implement a reconfigurable intelligent surface is to use a passive planar reflectarray (figure 2.2) whose antenna termination can be electronically controlled to shift the phase of the incident signal and properly backscatter it.

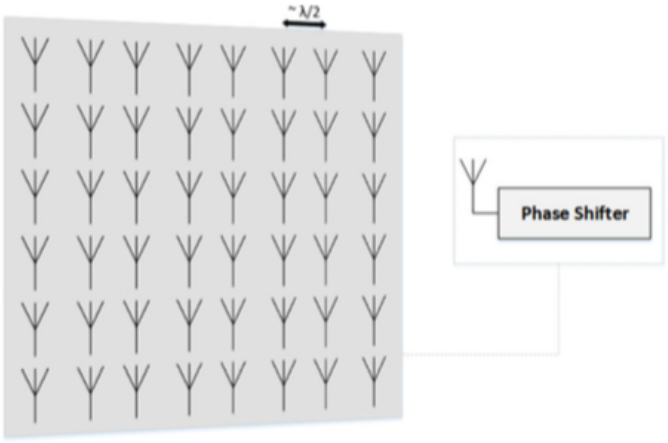

Figure 2.2: A 48-element reflectarray. Each element is a traditional antenna connected to a phase shifter [8].

When working at high frequencies, a large number of antennas is needed to obtain a surface of a few square meters. For example, considering a center band frequency equal to 28 GHz (the same of the 5G system), about ten

thousand antennas are needed to cover a surface of one square meters.

2) Metasurface-based RIS A more sophisticated implementation of a RIS can be made using metasurfaces [8]. A metasurface is the two-dimensional planar form of metamaterials, which are man-made synthetic materials with electromagnetic properties not found in naturally occurring materials. A metasurface is comprised of a large number of closely spaced deeply sub-wavelength resonating structures called pixels or meta-atoms.

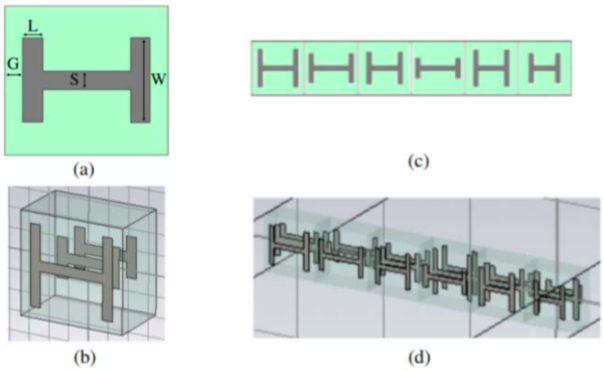

Figure 2.3: Metasurface scattering particles. a) Unit cell front view dog-bone shaped metallic particle. b) Unit cell perspective view with dielectric substrates made transparent for visualization. c) Supercell composed of 6 unit cells, front view. d) Supercell perspective view [9].

Both individual *meta-atom* (namely unit cell, depicted in figure 2.3) and the space between adjacent meta-atoms are much smaller than the wavelength. The meta-atom size and the thickness of the tile are important design factors that define the maximum frequency for electromagnetic (EM) wave interaction. According to [10], as a rule of thumb, meta-atoms are bounded within a square region of $[\frac{\lambda}{10}, \frac{\lambda}{5}]$. The minimal metasurface thickness is also in the region of $[\frac{\lambda}{10}, \frac{\lambda}{5}]$.
Furthermore, in order to make a metasurface reconfigurable, it is necessary to obtain dynamic meta-atoms able to change their electromagnetic properties through time (figure 2.4).

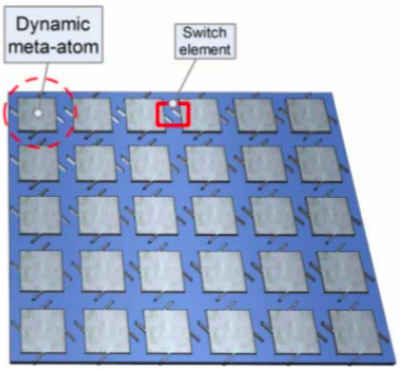

Figure 2.4: Dynamic metasurface: a very promising, cost-effective, and highly scalable approach is to control the metasurface switches as a diode array [9].

The very small size of these closely-packed atoms and their large number offer a vast number of degrees of freedom in manipulating the incident electromagnetic waves. However, the majority of empirical works in the literature employ reflectarray-based RIS. Even with the simpler reflectarray-based implementation, impressive results have been reported.

One crucial assumption for the linear channel model of RIS is the ignorance of any reflected signal coupling among neighbouring RIS elements. In practice, increasing the number of reflecting elements given the same RIS size is generally helpful in achieving more fine-grained passive beamforming and thus enhanced performance. This, however, will reduce the element spacing and may render the mutual coupling more severe and thus no more negligible, as nearby reflecting elements will interact with each other through their circuit coupling and thus result in coupled reflection coefficients.

2.2 Phase-shift control techniques

According to [7], to reconfigure RIS elements for highly controllable reflection, there are three main approaches proposed in the literature, namely:

1) mechanical actuation (e.g., mechanical rotation and translation of the RIS);

2) functional materials (e.g., liquid crystal and graphene);

3) electronic devices (e.g., positive-intrinsic-negative (PIN) diodes, field-effect transistors (FETs), or micro-electromechanical system (MEMS) switches).

In particular, the third approach (as the one depicted in figure 2.5) has been widely adopted in practical implementation both for reflectarray-based and metasurface-based RIS, due its fast response time, low reflection loss as well as relatively low energy consumption and hardware cost.
A typical architecture consists of three layers and a smart controller, as depicted in figure 2.5.

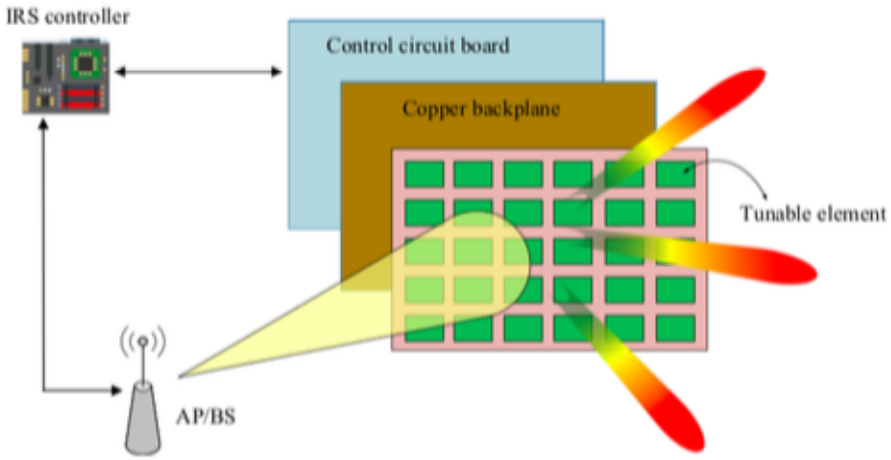

Figure 2.5: A typical architecture of a RIS based on electronic control [8].

The first/outside layer is composed of a large number of tunable (reconfigurable) metallic patches printed on a dielectric substrate to directly manipulate incident signals. In the second/intermediate layer, a copper plate is usually employed to minimize the signal energy leakage during RIS's reflection. It is followed by the third/inside layer that is a control circuit board responsible for exciting the reflecting elements as well as tuning their reflection amplitudes and/or phase-shifts in real-time. Moreover, the reflection adaptation is determined by a smart controller attached to each RIS, which can be implemented via field-programmable gate array (FPGA).
One example of an individual element's structure where a PIN diode is embedded in each element in order to control it, it is shown in figure 2.6.

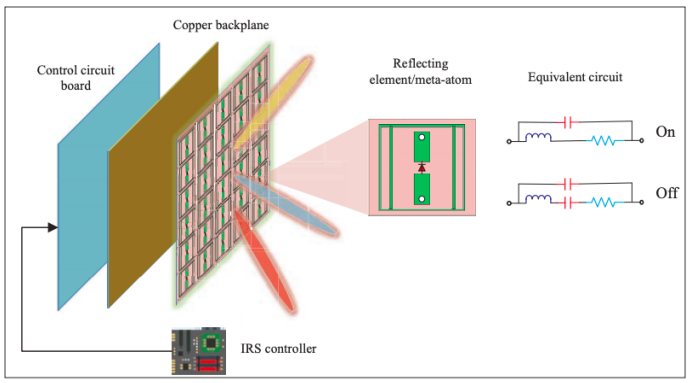

Figure 2.6: An example of the tunable reflecting element based on PIN diode [1].

By controlling its biasing voltage via a direct-current feeding line, the PIN diode can be switched between "ON" and "OFF" states as shown in the equivalent circuits reported in figure, thereby generating a phase-shift difference of π in rad.
The diode approach can be applied both for a reflectarray-based or for a metasurface-based RIS; in the latter, it can be applied also in a more complex structure (figure 2.7) where a meta-atom is seen as a supercell made up of a set of single units, as the one depicted in figure 2.3.

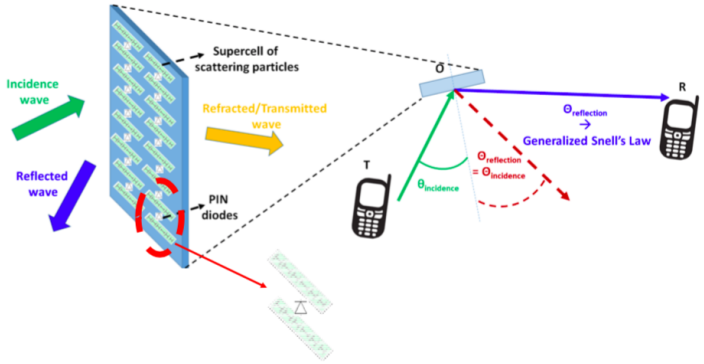

Figure 2.7: Reconfigurable metasurface with dynamic supercells [6].

The diode array approach results in a very simple control layer, which comprises just the wiring to connect each element switch to the gateway. Furthermore, the PIN diode switching frequency can be up to 5 MHz, which corresponds to the switching time of 0.2 microsecond. This is much smaller than the typical channel coherence time that is on the order of millisecond

and thus well suited for mobile applications with time-varying channels.
While continuously tuning the reflection amplitude and phase shift of each of the RIS's elements is certainly advantageous for communication applications, according to [7] it is costly to implement in practice because manufacturing such high-precision elements requires sophisticated design and expensive hardware, which may not be a scalable solution as the number of elements becomes very large. For example, to enable 16 levels of phase shift, four PIN diodes need to be integrated to each element. This not only makes the element design very challenging due to the limited element size, but also requires more controlling pins from the RIS controller to excite a large number of PIN diodes. As such, for practical RISs that usually have massive elements, it is more cost-effective to implement only discrete amplitude/phase-shift levels requiring a small number of control bits for each element, for example, 1-bit for two-level (reflecting or absorbing) amplitude control, and/or two-level (0 or π) phase-shift control. Furthermore, to reduce the hardware cost and design complexity, only discrete phase-shift control or discrete amplitude control may be implemented, thus leading to the following two special cases of the above discrete models:

1) RIS with discrete phase-shift control only, where for each reflecting element, only the phase-shift can be tuned while the reflection amplitude is set to its maximum value of one;

2) RIS with discrete amplitude control only, where for each reflecting element, only the reflection amplitude can be tuned while the phase-shift is set to be a constant (say, zero without loss of generality).

Generally speaking, phase-shift control (or phase beamforming) is of higher cost to implement as compared to amplitude control (or amplitude beamforming) for RIS, while the former can achieve better passive beamforming performance than the latter given the same number of control bits/discrete levels per reflecting element.
Although independent control of the reflection amplitude and phase shift simultaneously provides the maximum design flexibility, it imposes challenges for unit-cell design.

2.3 Models for RIS

Regardless of the adopted technology, a practical reflection model for RIS was proposed in [11] by modeling each antenna element as a resonant circuit with certain inductance, capacitance, and resistance, as shown in figure 2.8.

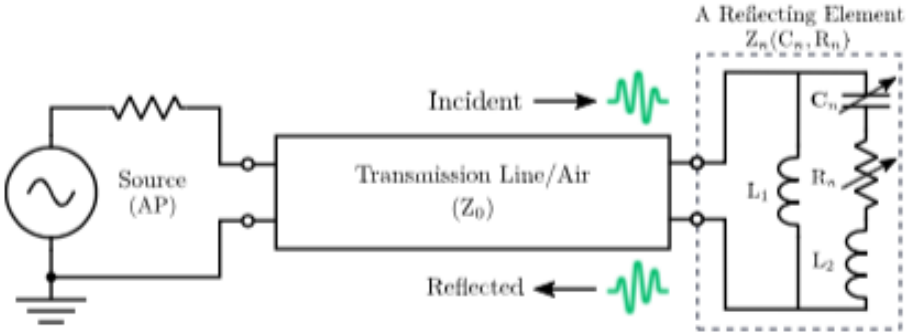

Figure 2.8: Equivalent transmission line model of a reflecting element [11].

Ideally, the reflection amplitude and phase-shift per element can be independently and continuously tuned.
The reflection amplitude typically attains its minimum value at the zero phase-shift, but monotonically increases and asymptotically approaches the maximum value of one as the phase-shift tends to -π or π. This is due to the fact that in each reflecting element, any phase-shift is achieved by tuning its effective capacitance/resistance, which inevitably changes the reflection amplitude.
To be specific, when the phase-shift approaches zero, the reflective currents (also referred to as image currents) are in-phase with the element currents, and thus the electric field as well as the current flow in the element are both enhanced, which results in maximum energy dissipation and the lowest reflection amplitude. In contrast, when the phase shift is around -π or π the reflective currents are out-of-phase with the element currents, and thus the electric field as well as the current flow in the element both diminish, thus leading to minimum energy loss and the highest reflection amplitude as shown in figure 2.9.

2.4 RIS in digital communication systems

In order to maximize the data rate and coverage, the controller has to optimize the RIS coefficients through appropriate algorithms. For this purpose, however, we must accurately know the status of the channel which also depends on the RIS configuration. Therefore, a critical aspect for the effective introduction of a RIS in a communication system is the channel estimation. One of the main challenge in RIS-enabled communication systems is the estimation of the channel state information (CSI), which depends on the channel

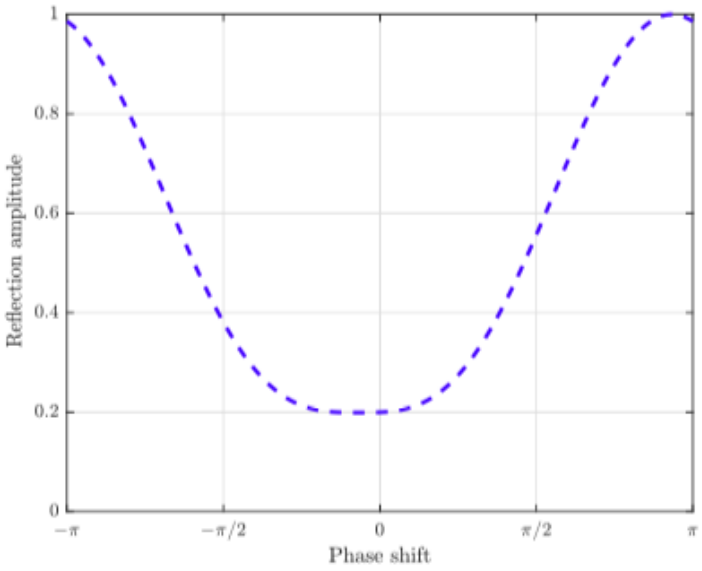

Figure 2.9: Reflection amplitude *vs* phase-shift for the practical RIS reflecting element [11].

between the transmitter and the RIS, the configuration of the RIS, and the channel between the RIS and the receiver. According to [7], however, in the existing literature there are two main approaches for RIS channel estimation based on two different RIS configurations, depending on whether it is mounted with sensing devices (receive RF chains) or not, termed as semi-passive RIS and (fully) passive RIS. The difficulty arises especially in the case of fully passive RISs that do not possess any active RF chains and thus cannot transmit pilot/training signals to facilitate channel estimation, which is in sharp contrast to the conventional wireless systems.

Semi-passive RIS To endow the RIS with sensing capability for channel estimation, additional sensing devices (such as low-power sensors) need to be integrated into the RIS, e.g., interlaced with RIS reflecting elements, as shown in figure 2.10, each equipped with a low-cost receive RF chain (e.g., low-resolution ADC) for processing the sensed signal. As such, the semi-passive RIS generally operates in one of the following two modes alternately over time:

1. ***Channel sensing mode*** *(phase I of the protocol illustrated in figure 2.10):* with all the reflecting elements turned OFF, the sensors are activated to receive the pilot signals from the BS/users in the down-

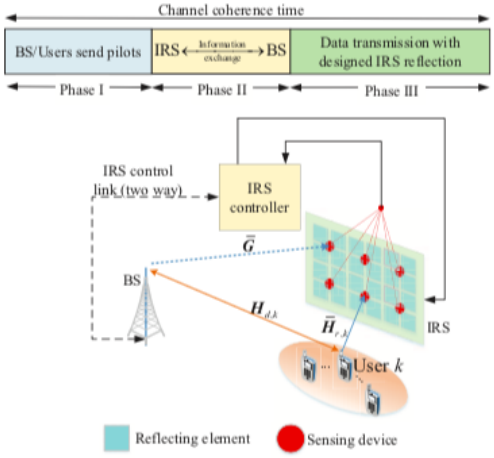

Figure 2.10: Semipassive RIS [7].

link/uplink for estimating their respective channels to RIS;

2. ***Reflection mode*** *(phase II of the protocol illustrated in figure 2.10):* with the sensors deactivated, the RIS reflecting elements are turned ON to reflect the data signals from the BS/users for enhancing the downlink/uplink communication, respectively.

Fully passive RIS To make the RIS energetically autonomous, as the one depicted in figure 2.11, it must be completely passive (without complicating the hardware with antennas for energy harvesting); this implies that it cannot be equipped with any active antenna capable of sending signals, making direct acquisition of CSI challenging.

A fundamental assumption of all the beamforming techniques studied in literature in order to guide properly the signal toward the receiver, is to have a complete knowledge of the propagation channel. In practice, the acquisition of accurate CSI of the RIS-reflected links is crucial, which, however, is a difficult task especially in a fully passive RIS, where the absence of sensors makes it more challenging. Moreover, to reduce the training overhead for RIS with practically large number of reflecting elements as well as simplify RIS reflection design for data transmission, an efficient approach is to group adjacent RIS elements (over which the RIS channels are usually spatially correlated) into a sub-surface, referred to as RIS element grouping; as a result, only the effective cascaded transmitter-RIS-receiver channel associated with

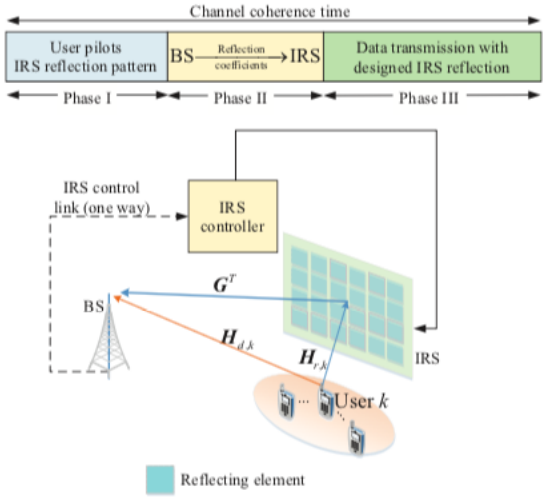

Figure 2.11: (Fully) passive RIS [7].

each sub-surface needs to be estimated, thus greatly reducing the training overhead. Thus, the element grouping strategy provides a flexible trade-off between training/design overhead/complexity and RIS passive beamforming gain in practice [7].
Note that although RIS only reflects signal without power amplification, it still needs a power supply to sustain the operation of reconfiguring the reflecting elements as well as its smart controller. The power consumption of the smart controller will depend on the controller's circuit implementation (e.g., FPGA) and communication module used. Therefore, RIS generally consumes substantially lower energy consumption than the existing active relays used for enhancing communications in wireless cellular networks.
Details on specific CSI methods for RIS will be illustrated in the next chapter.

Chapter 3

State of art of CSI estimation in RIS-enabled systems

In order to summarize the main approaches present in literature, it is important to note that the CSI estimation scheme depends on the particular setup of the system. In particular, it is possible schematize the main scenarios as following:

1. Semi-passive RIS or Fully passive RIS;
2. SISO or MISO/MIMO systems in single-user scenarios;
3. SISO or MISO/MIMO systems in multi-user scenarios;
4. Continuous or Discrete phase-shift.

1) Semi-passive or Fully passive RIS Regarding a semi-passive RIS, advanced signal processing tools, such as compressed sensing, data interpolation, and machine learning, can be applied to construct the CSI of transmitter/receiver-RIS links from the estimated CSI via the RIS sensors by exploiting their inherent spatial correlation. Moreover, it is worth noting that the channel estimation accuracy for semi-passive RIS is generally limited by the number of available sensors, their finite (e.g., 1-bit) ADC resolution, and the channel sensing time. Intuitively speaking, installing more sensors provides more channel-sensing measurements for reducing the RIS CSI construction error in general, applying higher-resolution ADCs can reduce the quantization error, and increasing the channel sensing time can help average out the sensing noise more effectively. However, according to [7], a systematic study on the fundamental limits, practical algorithms, and their cost-performance trade-offs for semi-passive RIS channel estimation is still

lacking in the literature, although a handful of preliminary works [12]–[16] on addressing some of these aspects have recently appeared.
When there are no sensors mounted on the RIS for low-cost implementation, RIS becomes fully passive and thus it is generally infeasible to acquire the CSI between the RIS and transmitter/receiver directly. In this (perhaps more practical yet challenging) case, an alternative approach is to estimate the cascaded transmitter-RIS-receiver channels; note that with this approach only the cascaded channels can be estimated, but it is also sufficient to control the RIS adequately during the communication phase. Moreover, it is worth pointing out that differently from the semi-passive RIS case where the channels need to be estimated via RIS sensors, the cascaded transmitter-RIS-receiver channel in the case of passive RIS can be directly estimated at the transmitter/receiver without the need of sophisticated channel reconstruction.
All the approaches discussed in the thesis have been developed under the assumption of fully passive RIS.

2) SISO or MISO/MIMO systems in single-user scenarios For the purpose of exposition, we proceed considering first the simple RIS-aided single-user system with flat-fading channels, where both the transmitter and receiver are equipped with one single antenna (SISO system). In this case, one practical method for RIS channel estimation is by employing an ON/OFF-based RIS reflection pattern [17], i.e., each one of the RIS elements is turned ON sequentially with the others set OFF at each time, thereby the cascaded channels associated with different RIS elements are estimated separately. Note that this method requires at least N pilot symbols for estimating the total N channel coefficients in this system. Albeit being simple to implement, the ON/OFF-based RIS reflection pattern incurs substantial reflection power loss as only one element is switched ON at each time and thereby the reflected signal is rather weak. To overcome this power loss issue and improve the channel estimation accuracy, the all-ON RIS reflection pattern can be employed, whereby all the N channel coefficients can be estimated over N pilot symbol durations [18].
For the passive RIS-aided single-user MISO/MIMO system, it is required to estimate more channel coefficients due to the increased channel dimensions and the matrix multiplication of the transmitter-RIS and RIS-receiver channels. By adopting the same approach applied in a SISO system for every antennas, the total training overhead is increased as compared to the single-user SISO case, which can be practically prohibitive if the number of the antennas is large. A lot of works in literature are based on the de-

composition and factorization of the channel matrix, in order to estimate the cascaded channel vectors. Anyway, given the large numbers of channels, certain RIS channel properties (such as low-rank, sparsity, and spatial correlation) can be exploited to facilitate the cascaded channel decomposition as well as reduce the training overhead [19]–[23]. Furthermore, to accelerate the training process, deep learning and hierarchical searching algorithms have also been developed for the channel estimation in passive RIS-aided MISO/MIMO systems [24]–[27].

3) SISO or MISO/MIMO systems in multi-user scenarios For channel estimation with passive RIS serving multiple users (with U users), a straightforward method is by adopting the single-user channel estimation design to estimate the channels of different users separately over consecutive time [28], which, however, increases the total training overhead by U times as compared to the single-user case and thus is practically prohibitive if the number of the users U is very large. Recall that all the users (receivers) share the same common transmitter-RIS channel, the training overhead for RIS channel estimation in the multi-user case can be significantly reduced. For example, a user can be selected as the reference user of which the cascaded channel is first estimated. Then, based on this reference CSI, the cascaded channels of the remaining $U-1$ users can be efficiently estimated by exploiting the fact that these cascaded channels are scaled versions of the reference user's cascaded channel and thus only the low-dimensional scaling factors, rather than the whole high-dimensional cascaded channels, need to be estimated.

4) Continuous or Discrete phase-shift In all the works of our knowledge present in literature, the CSI estimation schemes are based on the assumption of continuous values for RIS phase control, so that the optimization problem is not constrained and an optimal solution can be easily found. However, it is always possible to approximate the optimal solution with a sub-optimal considering as a generic phase coefficient of the RIS the one that comes closer to the optimal. This approach is usually valid both for approaches based on all-ON RIS reflection pattern and the ones based on machine learning techniques.

In this chapter, we illustrate a classical approach based on all-ON RIS reflection pattern [18], applicable in a single-user SISO system. Below, we also present an extension of this algorithm applicable in a MISO/MIMO system, based on the factorization of channel matrix [21].

3.1 Analysis of a CSI estimation scheme in a RIS-enabled SISO system

3.1.1 Introduction

As a first scenario, we consider an intelligent reflecting surface -aided single user system where a RIS with discrete phase shifts is deployed to assist the uplink communication. Both the BS and the user have a single antenna.

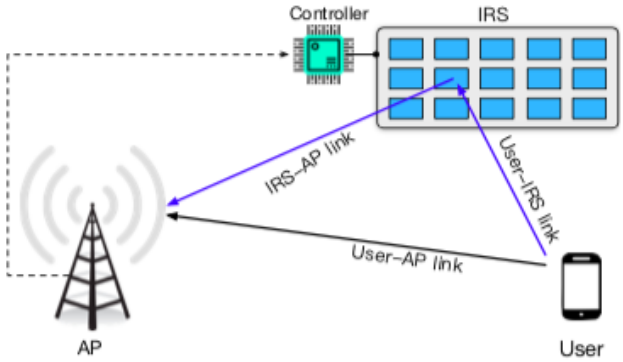

Figure 3.1: A RIS-aided single-user SISO communication system [18].

In order to illustrate CSI estimation schemes, we need to describe properly the channel model.
Since every cell of the RIS is made of N scattering element, then at the receiver the signal will be result of N different paths (not considering the direct one, without lose of generality). Under narrowband flat fading assumption, we can see the transmission channel as a vector of N complex numbers, each of them represents the complex channel coefficient between transmitter - a unit cell of the RIS - receiver. The same applies to the channel between the RIS and the receiver.
The goal is to estimate the cascaded channel vector.

3.1.2 Signal model

Starting from the hypothesis of flat fading and AWGN channel, we imagine to transmit a pilot signal x. The baseband equivalent signal at the receiver it is given by

$$y = x \cdot g + z \tag{3.1}$$

where $z \sim N(0, \sigma^2)$ represents the Gaussian noise component, and $g \in \mathbb{C}$ summarizes the global channel effect (that, for the hypothesis of flat fading, it attenuates and phase-shifts the signal sent). In particular, since y is given by the sum of every path at the receiver, assuming that the direct path is obstructed we can express g as follows:

$$g = \mathbf{h_{TR}} \mathbf{\Omega} \mathbf{h_{RU}} \tag{3.2}$$

where $\mathbf{h_{TR}} \in \mathbb{C}^{1\times N}$ and $\mathbf{h_{RU}} \in \mathbb{C}^{N\times 1}$ denote respectively the baseband equivalent channel between transmitter - RIS, and between RIS - user/ receiver, and $\mathbf{\Omega} = diag(\beta_1 e^{j\omega_1}, \beta_2 e^{j\omega_2}, \ldots, \beta_N e^{j\omega_N})$ takes into account the reflection coefficient of the RIS, where $diag(a_1, a_2, \ldots, a_n)$ represents the operator that generates a diagonal matrix of $N \times N$ dimensions, where the generic a_i element is collocated in the (i, i) position.
Defining in the same way the operator *diag* applied to a generic vector $\mathbf{v}$ of length l, $diag(\mathbf{v})$ generates a diagonal matrix of $l \times l$ dimensions, where the ith element of the vector is collocated in the (i, i) position of the matrix. So, let $\mathbf{h} \triangleq diag(\mathbf{h_{TR}})\mathbf{h_{RU}} \in \mathbb{C}^{N\times 1}$ denotes the cascaded user - RIS - receiver channel in the absence of RIS phase shifts, and $\boldsymbol{\theta} \triangleq [e^{j\omega_1}, e^{j\omega_2}, \ldots, e^{j\omega_N}] \in \mathbb{C}^{1\times N}$ denotes the RIS reflection vector imposing $\beta_i = 1, \forall i = 1, \ldots, N$. Then, we can rewrite (3.2) as

$$g = \boldsymbol{\theta}\mathbf{h} \tag{3.3}$$

[Note that the equation (3.3) is valid whatever the values of β.]
In order to estimate the channel $\mathbf{h}$, the transmitter sends N consecutive pilot symbols $x[n]$, $n = 1, 2, \ldots, N$ and the RIS changes its configuration such as at time n the configuration $\boldsymbol{\theta}[n]$ is adopted. Now, if we consider to send N consecutive pilot signals, we can extend and represent (3.1) under a matrix formulation. The received signal vector during this channel training can be compactly written as

$$\mathbf{y} = \mathbf{X}\mathbf{g} + \mathbf{z} \tag{3.4}$$

where $\mathbf{X} \triangleq diag(x[1], x[2], ..., x[N])$, $\mathbf{g} \triangleq [(g[1], g[2], ..., g[N]]^T$ and $\mathbf{z} \triangleq [(z[1],$ $z[2], ..., z[N]]^T$. Furthermore, we can write $\mathbf{g}$ as

$$\mathbf{g} = \mathbf{\Theta}\mathbf{h}$$

where $\mathbf{\Theta} \triangleq [\boldsymbol{\theta}[1], \boldsymbol{\theta}[2], \ldots, \boldsymbol{\theta}[N]]^T$ and where $g[n]$, $z[n]$, $\boldsymbol{\theta}[n]$ are respectively, the global channel coefficient, the noise term and the RIS reflection coefficients related to the transmission of the nth pilot signals $x[n]$ at time instant n.
Before proceeding, it is important to remember that usually RIS phases are not implemented using continuous phases between 0 and 2π, but they are

discrete and they can be represented using b bits of quantization. So, it is important to distinguish two cases:

1) when b is infinite;

2) when b it is limited and it is not possible to program the RIS in the optimal way.

3.1.3 Problem formulation

The final goal is to obtain a valid estimation of the vector $\mathbf{h}$ in order to the system could be able to predict how the cascaded channel g will be; a perfect knowledge of $\mathbf{h}$ permits to program the RIS coefficients in order to maximize the SNR at the receiver. In literature, some beamforming algorithms are studied in order to optimize the communication performance having only a noisy estimation of $\mathbf{h}$. So, let's proceed to analyze a possible way to get the CSI. An estimation of $\mathbf{g}$, denoted by $\hat{\mathbf{g}}$, can be derived from (3.4) as follows:

$$\hat{\mathbf{g}} = \mathbf{X^{-1}y} = \mathbf{g} + \mathbf{X^{-1}z} = \mathbf{g} + \mathbf{e_g} \tag{3.5}$$

Thus, if $\mathbf{\Theta}$ is of full-rank, the estimate of $\mathbf{h}$ is given by

$$\hat{\mathbf{h}} = \mathbf{\Theta}^{-1}\hat{\mathbf{g}} = \mathbf{h} + \mathbf{e_h} \tag{3.6}$$

where $\mathbf{e_g} \triangleq \mathbf{X^{-1}z}$ and $\mathbf{e_h} \triangleq \mathbf{\Theta}^{-1}\mathbf{X^{-1}z}$ denotes respectively the estimation error of $\mathbf{g}$ and $\mathbf{h}$. As such, the MSE of the above least square channel estimation is given by

$$\begin{aligned} \text{MSE} &= \mathbb{E}[||\mathbf{h} - \hat{\mathbf{h}}||^2] = \mathbb{E}[||\mathbf{e_h}||^2] \\ &= \mathbb{E}[tr(\mathbf{\Theta}^{-1}\mathbf{X}^{-1}\mathbf{z}\mathbf{z}^{\mathbf{H}}(\mathbf{X}^{-1})^H(\mathbf{\Theta}^{-1})^H)] \\ &= \frac{\sigma^2}{P_t} tr((\mathbf{\Theta}^H\mathbf{\Theta})^{-1}) \end{aligned} \tag{3.7}$$

where P_t denotes the transmit power associated to a generic symbol, and ^{H} represents the conjugate transpose operator.
The advantage of adopting the previous scheme is considerable, as the estimation error only depends on how the RIS is programmed. Now the goal becomes to find the best RIS configuration $\mathbf{\Theta}$ in order to minimize the MSE in (3.7).

3.1.4 Problem constraints

Accounting for the RIS discrete phase shifts and the feasibility of the previous estimation method, the constraints for the feasible RIS reflection pattern, $\boldsymbol{\Theta}$, are listed as follows.

1) The entries of the RIS reflection pattern should satisfy the constraints of unit-modulus and discrete phase, i.e.,

$$\begin{aligned} |[\boldsymbol{\Theta}]_{i,j}| &= 1, \qquad 1 \leq i \leq N, 1 \leq j \leq N \\ \angle([\boldsymbol{\Theta}]_{i,j}) &\in \mathbb{F}, \qquad 1 \leq i \leq N, 1 \leq j \leq N \end{aligned} \tag{3.8}$$

where $\mathbb{F}$ represents all the possible values that the phase coefficients can assume. Usually, $\mathbb{F} = \{0, \Delta\omega, ..., (K-1)\Delta\omega\}$ where $\Delta\omega = \frac{2\pi}{K}$ and $K = 2^b$.

2) The RIS reflection pattern should be full-rank, i.e.,

$$\text{rank}(\boldsymbol{\Theta}) = N \tag{3.9}$$

3.1.5 Problem optimization

Under the above constraints, the optimization problem for minimizing the MSE of channel estimation is formulated as

$$\begin{aligned} \text{(P1)} : &\min_{\boldsymbol{\Theta}} \frac{\sigma^2}{P_t} tr((\boldsymbol{\Theta}^H \boldsymbol{\Theta})^{-1}) \\ &\text{s.t. } (3.8) - (3.9) \end{aligned} \tag{3.10}$$

First, it can be easily verified that problem (P1) is always feasible, since there exists a naive reflection pattern that satisfies all the constraints in (3.8)-(3.9). We denote it by $\overline{\boldsymbol{\Theta}}$, whose entries are given by

$$[\overline{\boldsymbol{\Theta}}]_{i,j} = \begin{cases} -1, & i \neq j \\ 1, & \text{otherwise} \end{cases} \tag{3.11}$$

However, despite its feasibility, the objective function of (P1) is non-convex and the phase shifts of the RIS reflection pattern are restricted in a finite number of discrete values, turning the problem (P1) to be a NP-hard problem to solve. Numerically, the optimal solution to problem (P1) cannot be obtained by an exhaustive search over all possible reflection pattern: it is practically prohibitive try to find numerically the optimum since it increases

exponentially with N and/or b.
Focusing on the rank-related constraint (3.9), we can immediately think to consider an orthogonal matrix to overcome it, since an orthogonal matrix has surely maximum rank. Therefore, if there exists an orthogonal reflection pattern satisfying all the above constraints so that $\mathbf{\Theta}^H\mathbf{\Theta} = N\mathbf{I}_N$, then that it is surely an optimal solution to (P1), providing to the follow estimation error

$$\text{MSE} = \frac{\sigma^2}{P_t} tr((N\mathbf{I}_N)^{-1}) = \frac{\sigma^2}{P_t}$$

where $\mathbf{I}_N$ represents the $N \times N$ identity matrix.
In fact, if we look at the constraints (3.8) of the problem, we can not obtain a matrix $\mathbf{\Theta}^H\mathbf{\Theta}$ equal to $M\mathbf{I}_N$, with $M > N$. It follows that the minimum value of MSE expressed in (3.7) is reduced to

$$\text{MSE} = \frac{\sigma^2}{P_t}$$

due to the fact that $tr((\mathbf{\Theta}^H\mathbf{\Theta})^{-1})$ is greater to 1 (or equal, in the optimum configuration).

3.1.6 An optimal solution

Based on the previous considerations, an optimal orthogonal reflection matrix is given by the DFT matrix, denoted by $\overline{\mathbf{D}}$, whose entries are given by

$$[\overline{\mathbf{D}}]_{i,j} = e^{-j\frac{2\pi(i-1)(j-1)}{N}} \qquad 1 \leq i, j \leq N \tag{3.12}$$

In practical settings, we cannot always implement this matrix, because of the number b of available bits for the discrete phase shift levels. So the DFT matrix represents an optimal reflection pattern only for special cases. In particular, for RIS with equally spaced discrete phase shifts, the DFT matrix is an optimal solution if $N \in \{2^c$, where c = 1, 2, ...,b$\}$.

3.1.7 A sub-optimal solution

In order to obtain a quantized DFT matrix $\mathbf{D}$ for any N, it is proposed to design the matrix as follows:

$$[\mathbf{D}]_{i,j} = e^{j\varphi_{i,j}}$$

where $\varphi_{i,j} = arg\min_{\varphi_{i,j}} \mid e^{j\varphi_{i,j}} - e^{-j\frac{2\pi(i-1)(j-1)}{N}} \mid$.
It is important to say that now we have no guarantee of invertibility of $\mathbf{D}$,

but from extended simulations done by the authors of the article in question ([18]) we can observe that $\mathbf{D}$ is always invertible for $b \geq 2$ and achieves an MSE close to that of the continuous phase shifts when b is large.

3.1.8 Validity of the solution proposed for problem P1

In order to analyze the proposed estimation channel method for a SISO communication, we proceed testing the algorithm in different simulations.
First of all, we analyze the validity of the algorithm, comparing it with the "naive" approach (see equation 3.11). In particular, we have considered the following simulation parameters:

- transmitted power $P_t = 1$ Watt;
- number of reflecting elements $N = 100$;
- noise power σ^2 variable from [0.001, 0.1] Watt;

In order to analyze the validity of the optimal and sub-optimal solutions of the problem P1, we consider a random set of N complex numbers representing the CSI that has to be estimate through the tested algorithm.
The following results was obtained through Monte Carlo iterations, in which each problem is solved through different approaches: optimal, sub-optimal, "naive". From figure 3.2, we can note that with the optimal DFT matrix the MSE coincides with the theoretical result:

$$\text{MSE} = \frac{\sigma^2}{P_t}$$

We extend simulations considering noise power fixed to 0.1 Watt and changing the number of reflecting elements; in particular, we consider N variable in the interval [1,30]. The results are shown in the figure 3.3.

3.1.9 A method to lower the estimation error

If we imagine to send K pilot signals, with $K > N$, we can adapt the algorithm in a very simple way. In fact, it is sufficient to change the $\mathbf{\Theta^{-1}}$ matrix with the Moore-Pensore pseudo-inverse of $\mathbf{\Theta}$. In particular, we can adapt (3.6) with

$$\overline{\mathbf{h}} = \mathbf{\Theta}^{\dagger}\overline{\mathbf{g}} \tag{3.13}$$

where "†" refers to the operation of the pseudo-inversion of the matrix so that $\mathbf{\Theta}^{\dagger}$ represent the pseudo-inverse matrix of $\mathbf{\Theta}$. This operation works

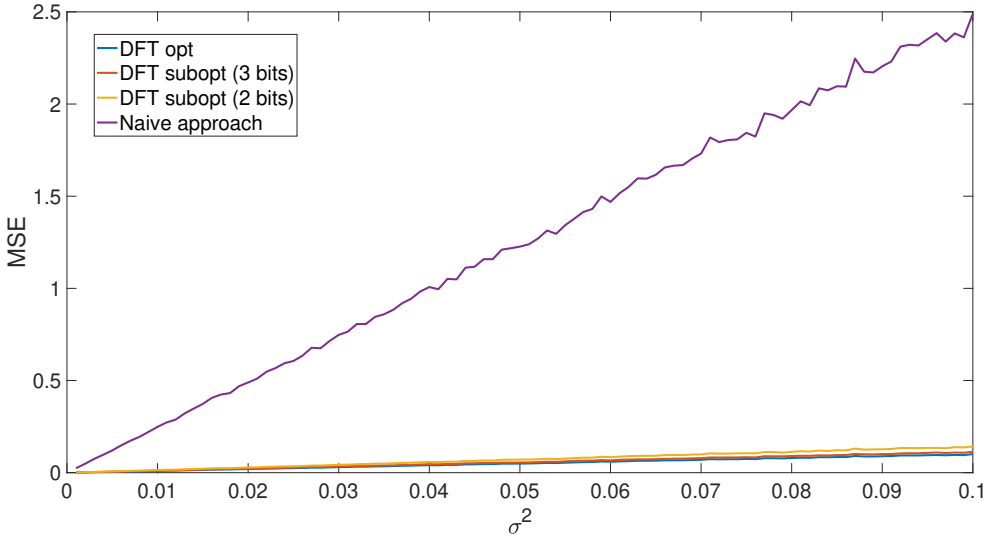

(a) Naive scheme vs optimal and sub-optimal solutions.

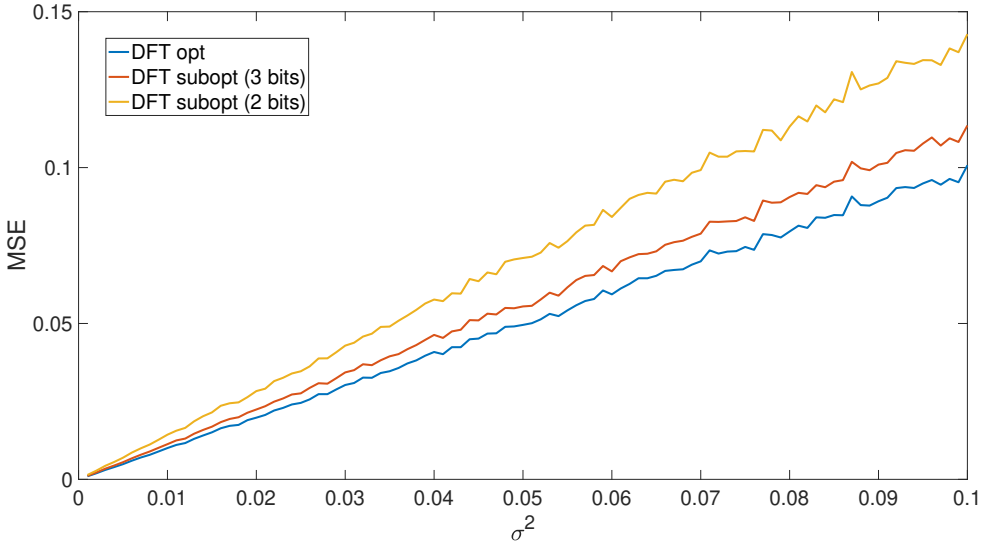

(b) Optimal vs sub-optimal solutions.

Figure 3.2: Simulations made with fixed number of RIS elements ($N = 100$).

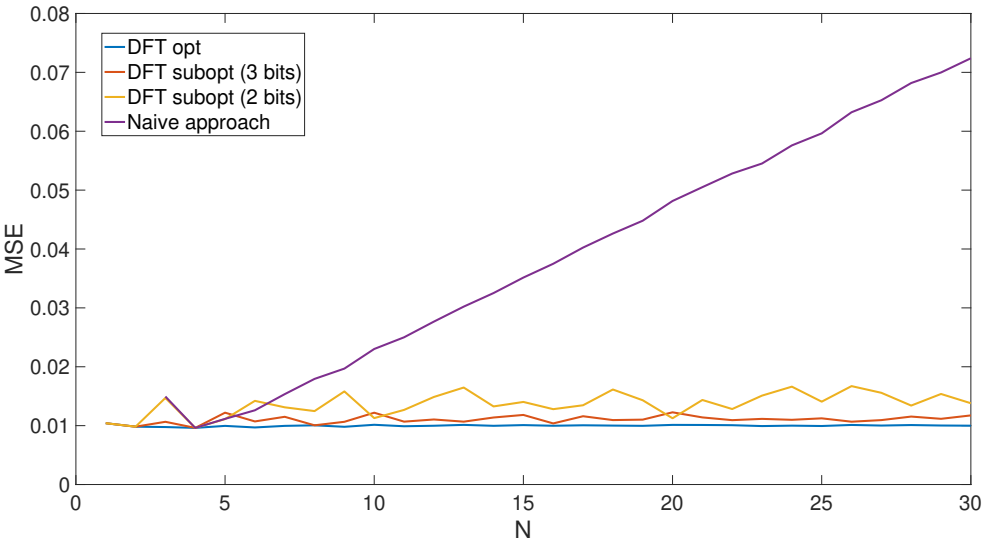

(a) Naive scheme vs optimal and sub-optimal solutions.

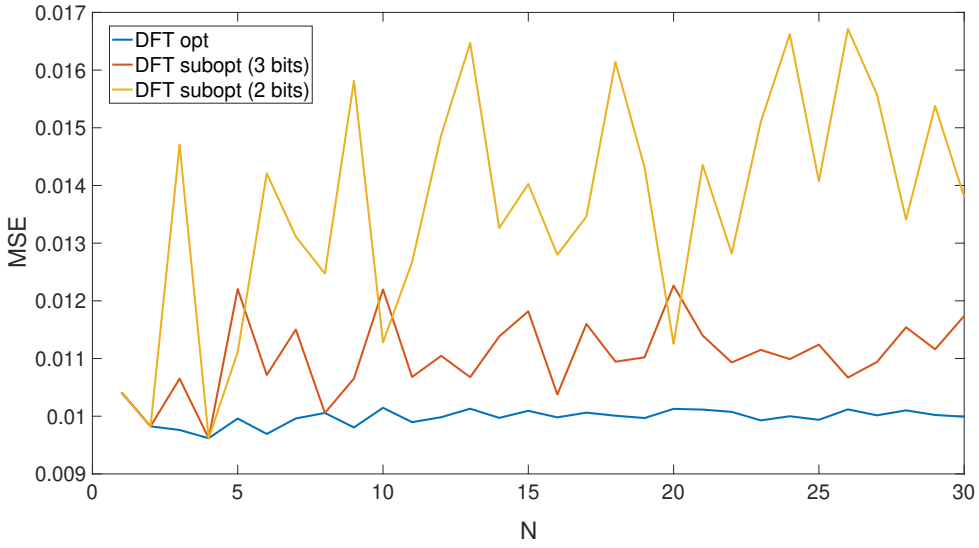

(b) Optimal vs sub-optimal solutions.

Figure 3.3: Simulations made with fixed noise power ($\sigma^2 = 0.1$ Watt).

because the matrix $\boldsymbol{\Theta}$ is a left-inverse, because it is a $K \times N$ matrix with maximum rank, such that $\boldsymbol{\Theta}^{\dagger}\boldsymbol{\Theta} = \frac{K}{N}\mathbf{I}_N$. If we consider (3.7), the estimation error expression become

$$MSE = \frac{\sigma^2}{P_t} tr(\boldsymbol{\Theta}^{\dagger}(\boldsymbol{\Theta}^{\dagger})^H) \tag{3.14}$$

If we design $\boldsymbol{\Theta}$ as a truncated DFT matrix, we obtain $tr(\boldsymbol{\Theta}^{\dagger}(\boldsymbol{\Theta}^{\dagger})^H) = \frac{N}{K}$. So, it follows that we can break down the estimation error simply considering to send a greater number of pilot signals rather than the total number of the RIS elements.

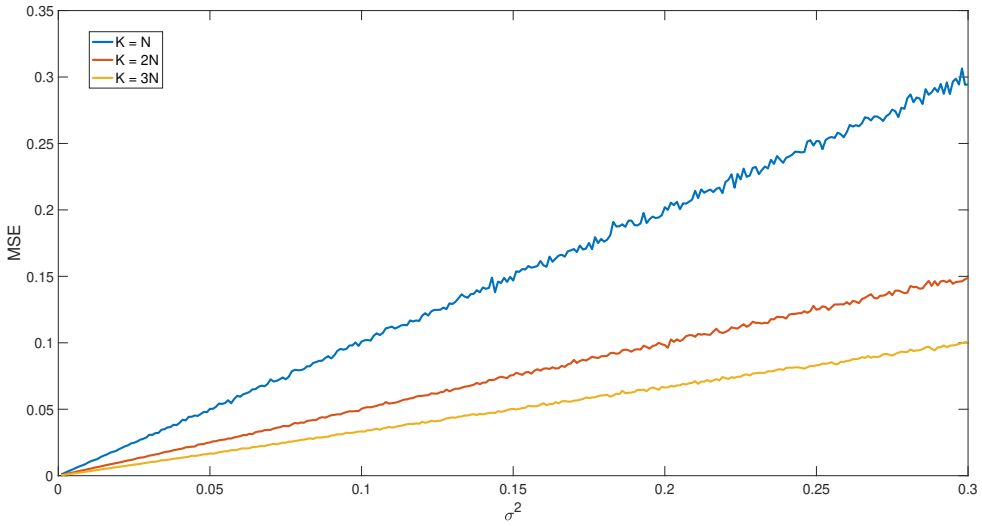

Figure 3.4: Simulation made exploiting the DFT configuration; the MSE results proportional to $\frac{N}{K}$.

3.2 Analysis of a CSI estimation scheme in a RIS-enabled MIMO system

3.2.1 Introduction

Now, we consider a MIMO communication system assisted by a RIS composed of N elements. The transmitter and the receiver are equipped with M and L antennas, respectively.

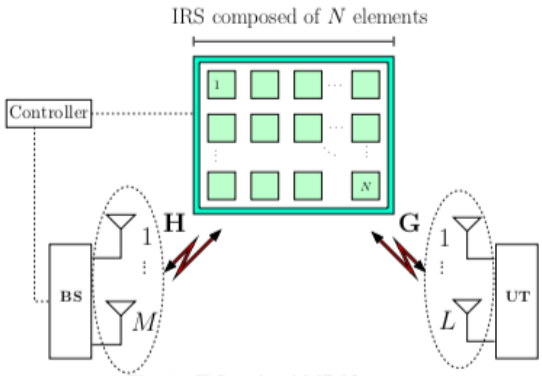

Figure 3.5: A RIS-aided single-user communication system [21].

In order to achieve the CSI, we need to describe properly the channel model.
We can see the transmission channel as a matrix of $L \times M$ complex numbers, where the generic (i, j) element represent the effect of the channel between the jth antenna of the transmitter and the ith antenna of the receiver.
Since every cell of the RIS is made up of a scattering element, for every signal sent by a single transmission antenna the receiver will experience N different paths (without loss of generality, we have neglected the direct path).
In the flat fading hypothesis, the goal is to estimate the channel matrix, where the real part of each (i, j) element represents the attenuation of the path between the jth antenna in transmission and the ith antenna of the receiver, while the imaginary one represents the phase shift.

3.2.2 Signal model

Starting to the hypothesis of flat fading and AWGN channel, we imagine to transmit a pilot signal $\mathbf{x} \in \mathbb{C}^{M\times 1}$. The baseband equivalent signal at the receiver it is given by

$$\mathbf{y} = \mathbf{C}\mathbf{x} + \mathbf{n} \tag{3.15}$$

where $\mathbf{n} \in \mathbb{C}^{L\times 1}$is the additive white Gaussian noise (AWGN) vector, and $\mathbf{C} \in \mathbb{C}^{L\times M}$ summarizes the global channel effect (that, for the hypothesis of flat fading, it is only about attenuation and phase shifting). In particular, since every element of $\mathbf{y}$ is given by the sum of every path came at the corresponding receiving antenna, we can express $\mathbf{C}$ as follow:

$$\mathbf{C} = \mathbf{G}\mathbf{D}\mathbf{H} \tag{3.16}$$

where $\mathbf{H} \in \mathbb{C}^{N \times M}$ and $\mathbf{G} \in \mathbb{C}^{L \times N}$ denote respectively the baseband equivalent channel matrix between transmitter - RIS, and between RIS - receiver, and $\mathbf{D} \in \mathbb{C}^{N \times N}$ represents $diag(\mathbf{s})$ (where $\mathbf{s} = [s_1 e^{j\omega_1}, s_2 e^{j\omega_2}, ..., s_N e^{j\omega_N}]$ takes into account the reflection coefficient of the RIS and $diag(\mathbf{s})$ refers to the diagonal matrix composed by $\mathbf{s}$ as the principal diagonal).
Now, if we consider to send T consecutive pilot signals, we can extend (3.13) representing the received signals during this channel training as

$$\mathbf{Y} = \mathbf{GDHX}^T + \mathbf{N} \tag{3.17}$$

where $\mathbf{X} = [\mathbf{x}[1], \mathbf{x}[2], ..., \mathbf{x}[T]]^T \in \mathbb{C}^{T \times M}$, $\mathbf{D} = diag(\mathbf{s})$ and $\mathbf{N} = [\mathbf{n}[1], \mathbf{n}[2], ..., \mathbf{n}[T]]^T$. For notation simplicity, we neglect the noise term and we focus only on the useful signal. We can rewrite the signal part of equation (3.15) as:

$$\overline{\mathbf{Y}} = \mathbf{GDZ}^T, \qquad \mathbf{Z} \triangleq \mathbf{XH}^T \in \mathbb{C}^{T \times N} \tag{3.18}$$

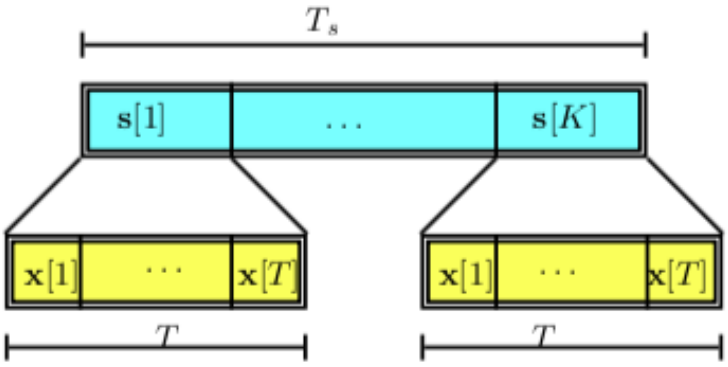

Figure 3.6: Training signals scheme [21].

If we imagine to repeat the transmission of the T pilot signals for K times (as depicted in figure 3.3), we can see the generic $\overline{\mathbf{Y}}[k]$ as the kth frontal matrix slice of a three way tensor $\overline{\mathcal{Y}} \in \mathbb{C}^{L \times T \times K}$ that follows a PARAFAC (PARallel FACtor) decomposition. Exploiting trilinearity of the parafac decomposition, we can unfold received signal tensor $\overline{\mathcal{Y}}$ in the following matrix forms:

$$\overline{\mathbf{Y}}_1 = \mathbf{G}(\mathbf{S} \diamond \mathbf{Z})^T \in \mathbb{C}^{L \times TK} \tag{3.19}$$

$$\overline{\mathbf{Y}}_2 = \mathbf{Z}(\mathbf{S} \diamond \mathbf{G})^T \in \mathbb{C}^{T \times LK} \tag{3.20}$$

where "$\diamond$" indicates the Khatri Rao product and $\mathbf{S} = [\mathbf{s}[1], \mathbf{s}[2], ..., \mathbf{s}[K]]$.

3.2.3 Problem formulation

The goal is to estimate $\mathbf{G}$ and $\mathbf{H}$ from the received signals.
From the noisy versions of the matrix unfoldings (3.17) and (3.18), we can derive an iterative solution based on a Bilinear Alternating Least Squares (BALS) algorithm. This algorithm consists of estimating the matrices $\mathbf{G}$ and $\mathbf{H}$ in an alternating way by iteratively optimizing the following two cost functions:

$$\overline{\mathbf{G}} = arg\min_{\mathbf{G}} ||\mathbf{Y}_1 - \mathbf{G}(\mathbf{S} \diamond \mathbf{X}\mathbf{H}^T)^T||_F^2 \tag{3.21}$$

$$\overline{\mathbf{H}} = arg\min_{\mathbf{H}} ||\mathbf{Y}_2 - \mathbf{X}\mathbf{H}^T(\mathbf{S} \diamond \mathbf{G})^T||_F^2 \tag{3.22}$$

the solutions of which are respectively given by

$$\overline{\mathbf{G}} = \mathbf{Y}_1[(\mathbf{S} \diamond \mathbf{X}\mathbf{H}^T)^T]^\dagger \tag{3.23}$$

$$\overline{\mathbf{H}}^T = \mathbf{X}^\dagger\mathbf{Y}_2[(\mathbf{S} \diamond \mathbf{G})^T]^\dagger \tag{3.24}$$

where $||\ ||_F$ refers to the norm operator.
The BALS algorithm can be summarized as follows:

1. Let i the ith iteration of the algorithm, and set $i = 0$;
2. At the first iteration, initialize randomly the matrix $\overline{\mathbf{H}}_{(i=0)}$, where the subscript i indicates the matrix at the ith iteration;
3. Increment $i = i + 1$;
4. Find a least square estimate of G, at the iteration i:

$$\overline{\mathbf{G}}_{(i)} = \mathbf{Y}_1[(\mathbf{S} \diamond \mathbf{X}\mathbf{H}_{i-1}^T)^T]^\dagger \tag{3.25}$$

5. Find a least square estimate of H, at the iteration i:

$$\overline{\mathbf{H}}_{(i)}^T = \mathbf{X}^\dagger\mathbf{Y}_2[(\mathbf{S} \diamond \mathbf{G}_i)^T]^\dagger \tag{3.26}$$

6. Repeat steps 3 to 5 until converge.

Despite the iterative nature of the BALS algorithm, only a few iterations are necessary for convergence (usually less than 10 iterations) due to the knowledge of the matrix factor $\mathbf{S}$ that remains fixed during the iterations.
Provided that the above conditions are satisfied, the channel estimates $\overline{\mathbf{G}}$ and $\overline{\mathbf{H}}$ are unique up to scalar ambiguities. More specifically, the rows of $\overline{\mathbf{H}}$ and the columns of $\overline{\mathbf{G}}$ are affected by scaling factors that compensate each

other, i.e., $\overline{\overline{\mathbf{H}}} = \boldsymbol{\Delta}_H \mathbf{H}$ and $\overline{\mathbf{G}} = \mathbf{G}\boldsymbol{\Delta}_G$, where $\boldsymbol{\Delta}_H \boldsymbol{\Delta}_G = \mathbf{I}_N$. However, these ambiguities disappear when building an estimate of the cascaded (end-to-end) channel $\mathbf{C} = \overline{\mathbf{G}}\ \overline{\mathbf{H}}^T$ of the RIS-assisted MIMO system. Note also that permutation ambiguity does not exist due to the knowledge of the RIS matrix $\mathbf{S}$ at the receiver.

The only constraints are about the possibility to construct all the inverse matrix above mentioned. So, the BALS method requires that $(\mathbf{S} \diamond \mathbf{X}\mathbf{H}^T) \in \mathbb{C}^{KT \times N}$ and $(\mathbf{S} \diamond \mathbf{G}) \in \mathbb{C}^{KL \times N}$ have full column-rank, so that the problems (7), (8) admit unique solutions. This implies that $min(KT, KL) \geq N$.

Chapter 4

A novel algorithm for overhead reduction

If we imagine to send K pilot signals, with $K < N$, it is not possible to exploit the same approach previously analyzed. In fact, if $K < N$, the RIS coefficients' matrix $\mathbf{\Theta}$ will result a right-inverse matrix, making impossible the CSI estimation through equation (3.6).
In this chapter we are going to present a novel algorithm able to obtain a valid channel estimation exploiting the characteristics of the channel itself. In particular, in the next sections, we are going to analyze the phase profile of the cascaded channel $\mathbf{h}$ as a function of the position of the transmitter and receiver, under both far-field and near-field hypothesis, and then how this information can be exploited thanks to the maximum likelihood criterion (ML) in order to get a valid CSI estimation.
Let us proceed to illustrate the considered scenario:

- Transmitter, receiver and RIS placed in a 10 meters $\times$ 10 meters room, at the same altitude ($z = 1$);
- Center frequency of the signal equal to 28 GHz, to which a wavelength $\lambda = 1$ cm corresponds;
- Transmitter placed at a corner of the room, in $(x = 0, y = 10, z = 1)$;
- Receiver placed at the opposite corner of the room, in $(x = 10, y = 10, z = 1)$;
- Stripe RIS composed of $N = 100$ antennas equally spaced by a half of wavelength λ, placed along x dimension at $(y = 0, z = 1)$. The first element is placed at $(x = 2, y = 0, z = 1)$ and the last one at $(x = 2.535, y = 0, z = 1)$ (being the RIS 0.535 meters long).

The described scenario is depicted below, in figure 4.1.

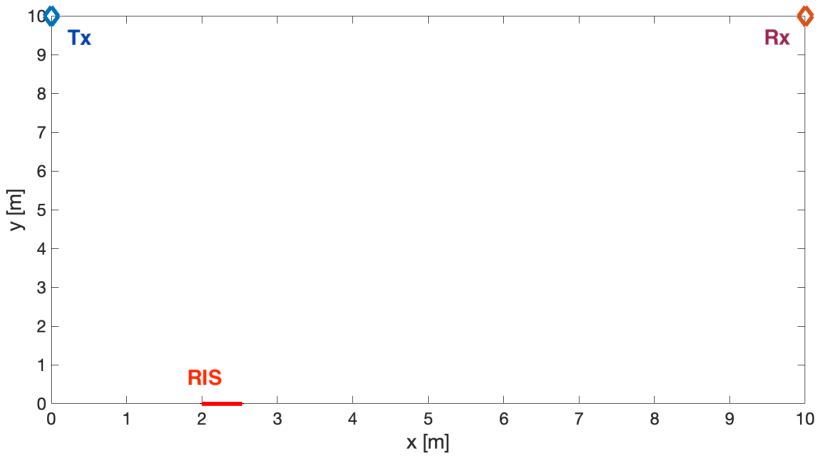

Figure 4.1: Illustration of the scenario.

4.1 RIS-assisted communication in far-field

4.1.1 Phase profile of the cascaded channel vector

When the transmitter is placed far enough from the RIS, it is possible to approximate the wave front of the EM field impinging to every element of the surface as a plane wave, as shown in figure 4.2.

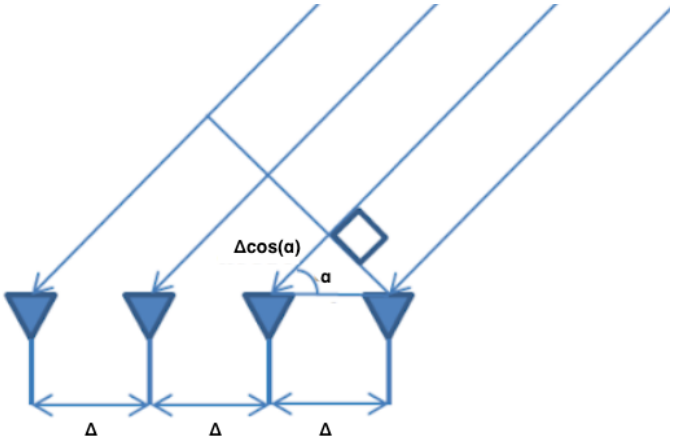

Figure 4.2: Wave front of the EM field transmitted toward RIS's elements, in far-field communication.

In this particular condition, the angles of incidence of the impinging wave front at each antenna are the same. In the hypothesis of line-of-sight (LOS) between transmitter and RIS and without considering the multipath effect of the surrounding environment, it follows that the generic channel $\mathbf{h_{TR}} = [h_{TR_1}, h_{TR_2}, \ldots, h_{TR_N}]$ between transmitter and RIS must be given by the following expression:

$$h_{TR_n} = q_{1_n} \cdot e^{i\frac{2\pi}{\lambda}\cdot\Delta\cdot(n-1)\cdot sin(\alpha)}, \quad \forall n = 1, \ldots N, \tag{4.1}$$

where the index n represents the path toward the nth reflecting element of the RIS, q_{1_n} the channel gain of the respective path (that thanks to the far-field hypothesis we can assume to be constant, and equal to $q_1 = \sqrt{\frac{G_t\cdot\lambda^2}{(4\pi)^2}} \cdot \frac{1}{d_1}$, where G_t is the transmitter antenna's gain and d_1 the distance between the transmitter and the RIS), i the imaginary unit, Δ the inter-element spacing and α the angle of incidence of the EM field impinging the RIS. It is also important to note that the term $sin(\alpha)$ corresponds to the phase gradient of the channel $\mathbf{h_{TR}}$ along the RIS and that it remains constant for all the vector.
It is now clear that in far-field communication it is sufficient to know the value of the sine of the angle of incidence α of the wave front and the distance between every element of the surface to characterize uniquely the channel vector $\mathbf{h_{TR}}$ (with the exception of constant q_1 relating to the path loss).
Given the position of the transmitter, because of in far-field hypothesis the RIS is seen as a point, we can say that α is also the angle between transmitter and the RIS itself; by considering also the receiver in far-field and following the same steps, we can refer to β as the angle between the RIS and the receiver. It follows that also the channel $\mathbf{h_{RU}} = [h_{RU_1}, h_{RU_2}, \ldots, h_{RU_N}]$ can be expressed as:

$$h_{RU_n} = q_2 \cdot e^{i\frac{2\pi}{\lambda}\cdot\Delta\cdot(n-1)\cdot sin(\beta)}, \quad \forall n = 1, \ldots N, \tag{4.2}$$

where $q_2 = \sqrt{\frac{G_r\cdot\lambda^2}{(4\pi)^2}} \cdot \frac{1}{d_2}$ and G_r and d_2 represents respectively the receiver antenna's gain and the distance between the RIS and the receiver.
For this reason, the cascaded channel vector $\mathbf{h}$, that it is equal to the product element by element of the two vectors $\mathbf{h_{TR}}$ and $\mathbf{h_{RU}}$, is:

$$h_n = k \cdot e^{i\frac{2\pi}{\lambda}\cdot\Delta\cdot(n-1)\cdot(sin(\alpha)+sin(\beta))}, \quad \forall n = 1, \ldots N, \tag{4.3}$$

where $k = q_1 \cdot q_2$ is the total path loss effect.
In order to see if the assumption of far-field is valid at least when the transmitter and receiver are placed at a sufficient distance from the RIS in the

previously described scenario, we are going to consider the scenario depicted in figure 4.1.
Plotting the phase profile and the phase gradient of the cascaded channel in those particular positions of transmitter and receiver, we obtain the results shown in figure 4.3.

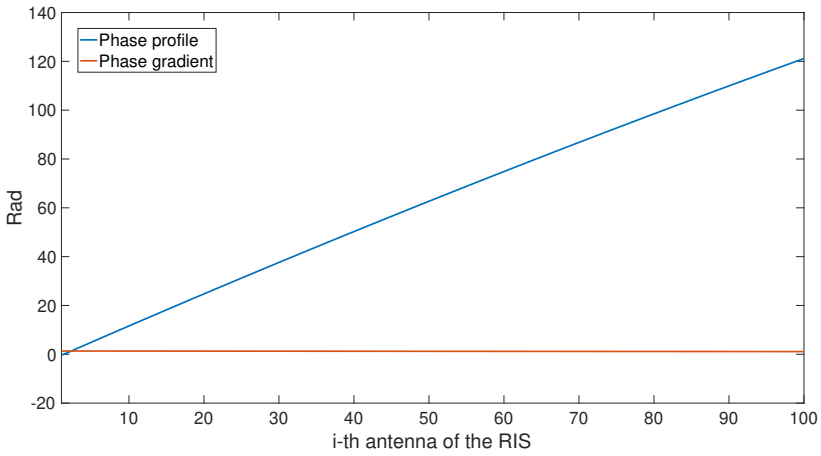

Figure 4.3: Phase profile and phase gradient of the vector **h** with transmitter and receiver far from the RIS.

Remembering that in far-field hypothesis we would have expected a constant phase gradient, and consequently a linear phase profile, we can note from figure 4.3 that, in those particular positions of transmitter and receiver, the far-field hypothesis seems to be perfectly satisfied. Anyway, making a zoom of the only gradient profile, we can note that it varies from [1.35, 1.11] rad about; we can therefore approximate it as a constant without large error.

Optimal configuration of the RIS in far-field communications During the communication phase, the best configuration of the RIS coefficients consists in setting up $\boldsymbol{\theta}$ as the conjugate of the cascaded vector **h**, in such a way that all reflected components sum up coherently at the receiver side. For this reason, we can refer to the term $sin(\alpha) + sin(\beta)$ as the absolute value of the optimal phase gradient of the RIS.
Considering that the phase gradient of the cascaded channel **h** depends on the positions of the transmitter and the receiver (because it depends on α and β), we can extend the previous simulation by varying the x dimension of the receiver, keeping fixed ($y = 10, z = 1$) and the position of the transmitter. From figure 4.4, we can note that the phase gradient of the cascaded channel depends linearly on $sin(\alpha) + sin(\beta)$. In particular, we can note that

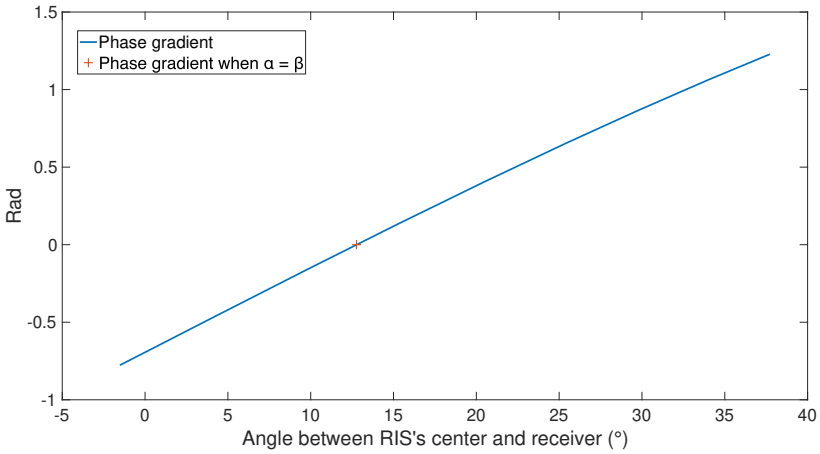

Figure 4.4: Phase gradient of the vector $\mathbf{h}$ as a function of receiver position.

when $\alpha = \beta$, the gradient assumes a value equal to zero. It follows that, in far-field communications, a RIS programmed with the optimal coefficients behaves like an anomalous mirror whose angle is such that the signal is reflected towards the receiver. Because of the RIS is fixed along a wall, it can be seen as an intelligent mirror able to overcome the law's Snell of reflection simply re-programming its coefficients.

4.1.2 Channel maximum likelihood estimator

Keeping in mind the geometry of the problem, through the gradient estimation it is possible to calculate the whole channel $\mathbf{h}$. It is important to note that theoretically we can proceed exploiting the optimal method shown in the Chapter 3 with only two pilot signals: in fact, the constant gradient could be estimated only by two measures. The problem of this approach is that we would need to select two reflecting elements and get an estimate one by one, keeping only one element ON at a time, making the received power extremely low. For this reason, we can get around the problem by changing our approach. In particular, we can search (e.g., by considering more measurements obtained considering a subset of the possible RIS configurations) for the estimate of the phase gradient of the cascaded channel that minimizes the error between the collected measurements and the expected receiver vector which depends on the channel $\mathbf{h}$ and the RIS configuration $\boldsymbol{\Theta}$. In order to apply the ML criterion to find an estimate of $\mathbf{h}$, because of Δ is fixed and equal to $\frac{\lambda}{2}$, the problem can be reduced to the research of the

$sin(\alpha) + sin(\beta)$. The problem to solve becomes:

$$\hat{s} = \arg\min_{s} \mid \mathbf{y} - \mathbf{X}\boldsymbol{\Theta}\mathbf{h}(s) \mid \tag{4.4}$$

where $s = sin(\alpha) + sin(\beta)$, $\hat{s}$ an its estimate and $\mathbf{h}(s)$ the cascaded channel vector in function of the gradient (see expression (4.3)).

ML estimation scheme The ML criterion is based on the approach described in the flow chart described in figure 4.5. Points from 3 to 5 are iterated for different values of s. Trying theoretically all possible values of s, the receiver can consider as the best estimate of the cascaded channel vector the $\mathbf{h_{test}}$ that produced the lowest norm e. It is important to note that because of we do not know the transmitter and the receiver position we are not able to know the path loss effect; for this reason, the term e is calculated normalizing $\hat{\mathbf{g}}$ and $\mathbf{g_{test}}$.
In order that this approach produces a good estimate of $\mathbf{h}$ it is necessary that:

- The number of values of s tested during the ML search is sufficiently large;
- The link budget is adequate, in order that $\hat{\mathbf{g}}$ is not too corrupted by the noise.

In section 4.3 the validity of this approach will be assessed through simulation results.

4.2 RIS-assisted communication in near-field

4.2.1 Phase profile of the cascaded channel vector

A more detailed expression of the channel between the transmitter and the RIS can be obtained approximating the phase gradient as a linear function, recalling figure 4.3. In particular, taking into account that a linear gradient is equivalent to a parabolic phase profile, we obtain:

$$h_{TR_n} = q_{1_n} \cdot e^{i\frac{2\pi}{\lambda}\cdot\Delta\cdot(n-1)\cdot sin(\alpha)+i\frac{2\pi}{\lambda}\cdot\frac{(\Delta\cdot(n-1))^2}{2\cdot dF_{TR}}}, \quad \forall n = 1, \dots N, \tag{4.5}$$

where dF_{TR} (the focal distance) represents the distance between the transmitter and the center of the RIS.
The same is for the channel between the RIS and the receiver:

$$h_{RU_n} = q_{2_n} \cdot e^{i\frac{2\pi}{\lambda}\cdot\Delta\cdot(n-1)\cdot sin(\beta)+i\frac{2\pi}{\lambda}\cdot\frac{(\Delta\cdot(n-1))^2}{2\cdot dF_{RU}}}, \quad \forall n = 1, \dots N, \tag{4.6}$$

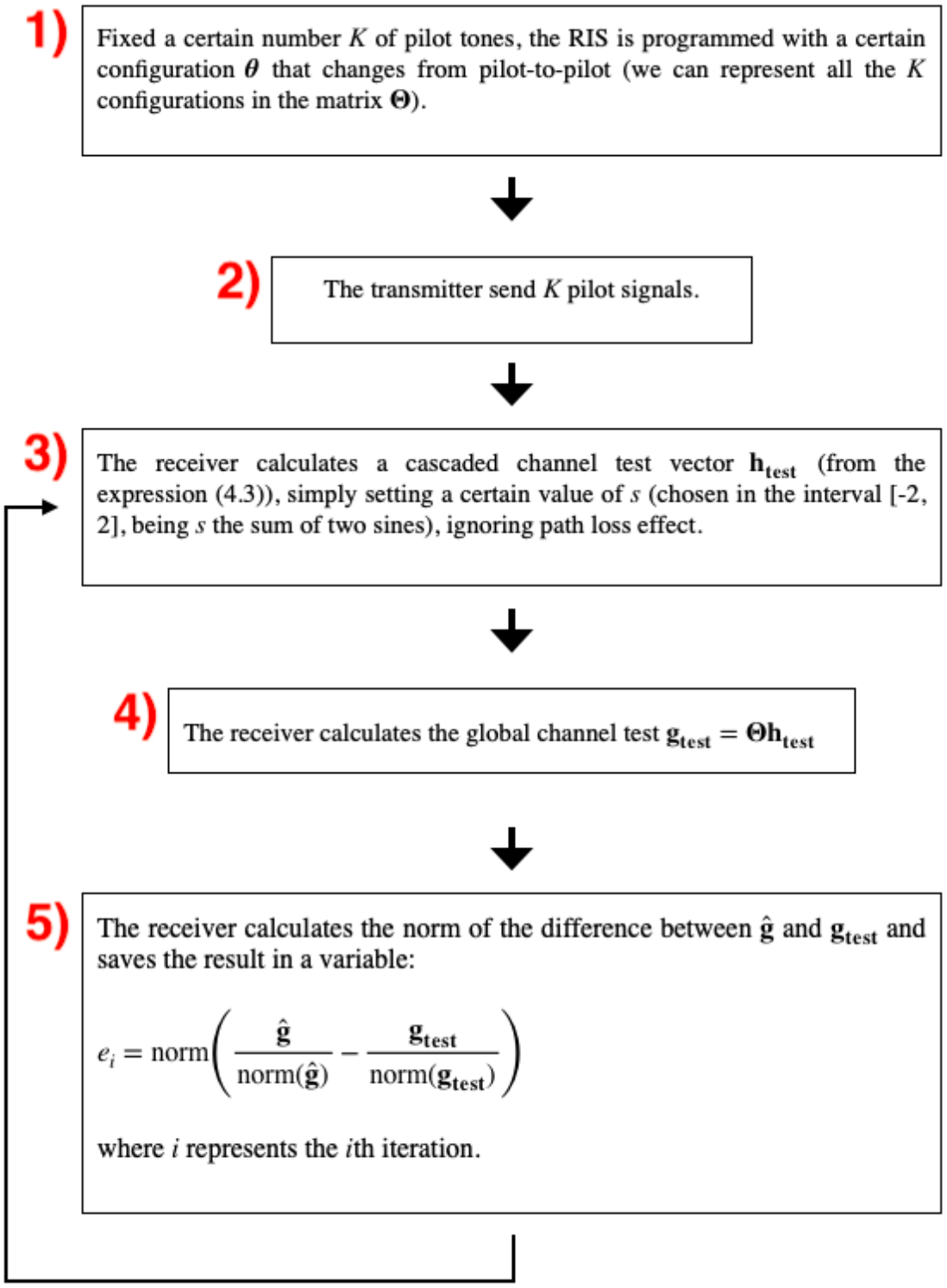

Figure 4.5: Description of the ML criterion adopted in order to estimate the cascaded channel $\mathbf{h}$.

where dF_{RU} represents the distance between the center of the RIS and the receiver.
It follows that the cascaded channel $\mathbf{h}$ is given by:

$$h_n = k \cdot e^{i\frac{2\pi}{\lambda}\cdot\Delta\cdot(n-1)\cdot(sin(\alpha)+sin(\beta))+i\frac{2\pi}{\lambda}\cdot\frac{(\Delta\cdot(n-1))^2}{2\cdot dF}}, \quad \forall n = 1, \dots N, \tag{4.7}$$

where $\frac{1}{dF} = \frac{1}{dF_{TR}} + \frac{1}{dF_{RU}}$. Note that in this case the knowledge of the only term $sin(\alpha) + sin(\beta)$ is not enough to characterize uniquely the cascaded channel vector. In particular, we can describe uniquely a parabolic profile (as the one expressed by equation (4.7)) through the knowledge of the term relating to the angles α and β and the cascaded distance dF.

4.2.2 Channel maximum likelihood estimator

The approach is the same of the one proposed in the subsection 4.1.2 (figure 4.5), but in this case we have to do a joint search, one for the term referring to $sin(\alpha) + sin(\beta)$ and one for the focal distance dF.

4.3 Implementation and validation of the ML approach

Recalling that our ML-based approach is valid when the estimation of $\mathbf{g}$ is not too corrupted by the noise, we are going to consider a scenario where thanks to an adequate link budget we can ensure high SNR at the receiver. Taking a cue from the link budget proposed in the article [29], we are going to fixed following data:

- Transmitted power P_t [dBW] = 0;
- Transmitter antenna gain G_{tx} [dB] = 5;
- Signal bandwidth W = 10 MHz;
- Center frequency f_c = 28 GHz;
- Receiver antenna gain G_{rx} [dB] = 2;
- Receiver noise figure F [dB] = 3;
- Reference temperature of receiver T = 290 °C;

From these data is possible to calculate the noise power σ^2 as $N_0 \cdot W$, where $N_0 = 1.38 \cdot 10^{-23} \cdot T \cdot F$.

Far-field hypothesis We begin our simulations considering a generic transmitter and receiver position, for example transmitter placed in $(x = 10, y = 0, z = 1)$ and receiver in $(x = 10, y = 10, z = 1)$ (figure 4.1). In order to evaluate the ML criterion, we consider a large number of test values for s, for example equal to 1000. In fact, considering that s represents a sum of two sines, it can only assume a value included in the interval [-2,2] and trying 1000 possible values means making a search with a very fine step. Furthermore, in our scenario, it is possible to consider a narrower range, for example [-1,1]. We can now apply the ML criterion to the considered scenario, in order to analyze its performance as a function of the number of pilot tones and compare it with the ideal case with a perfect CSI estimation.
Since setting up $\boldsymbol{\theta}$ as the conjugate of $\hat{\mathbf{h}}$ may not be the optimal solution for imperfect CSI, in literature beamforming techniques have been proposed in order to minimize the effect of the estimation error. Anyway, in our simulations, we exploit the optimum approach considering the estimate $\hat{\mathbf{h}}$ obtained through ML criterion, evaluating the performance in comparison with the case of perfect knowledge of CSI.
The following simulations show the comparison between the SNR achievable at the receiver (defined as the ratio between the received power and the thermal noise σ^2) in three cases:

- Perfect CSI estimation (where the received power is maximized);
- Imperfect CSI estimation;
- Unconfigured RIS (where RIS's coefficients assume random values during the communication phase).

Setting a random training coefficients of the RIS for the estimation phase of the channel and making the assumption of far-field communication, we obtain the results shown in figure 4.6. Always considering the same position for the transmitter and the receiver, it is interesting to note if also in this approach, based on ML criterion, the DFT-based training coefficients can give us better results. Considering the comparison between figures 4.6 and 4.7, by repeating the simulation for different transmitter and receiver positions same results are obtained. In particular, it is clear that:

- Both approaches come to the convergence;
- The DFT-based training pattern causes an "ON/OFF" behavior before and after 10-15% about of pilot tones.

For this reason, from here on all the simulations will be made taking into account a RIS configured with a random pattern for the estimation phase of

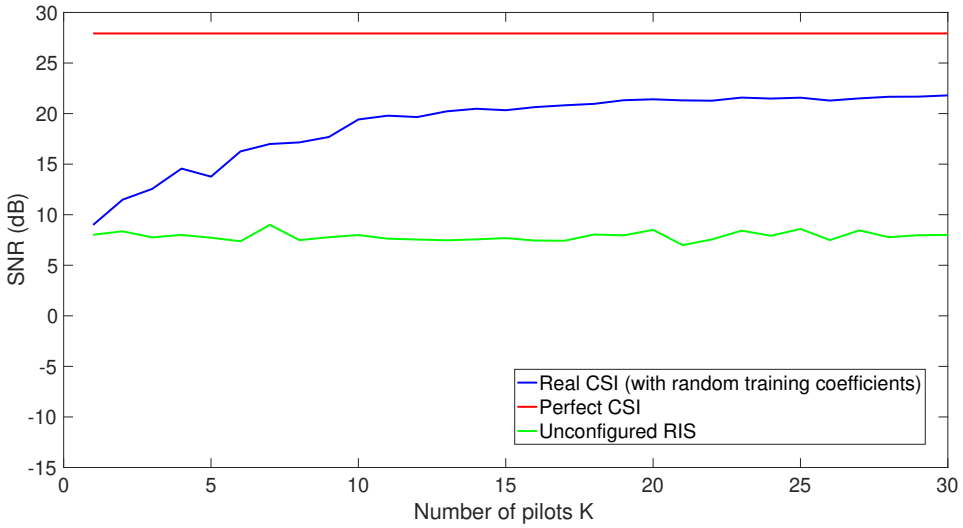

Figure 4.6: Results obtained exploiting the ML criterion (with 1000 iterations and setting the RIS with a random training pattern during the estimation phase of the channel). Simulations are made considering 100 Monte Carlo iterations, in order to mediate the noise effect.

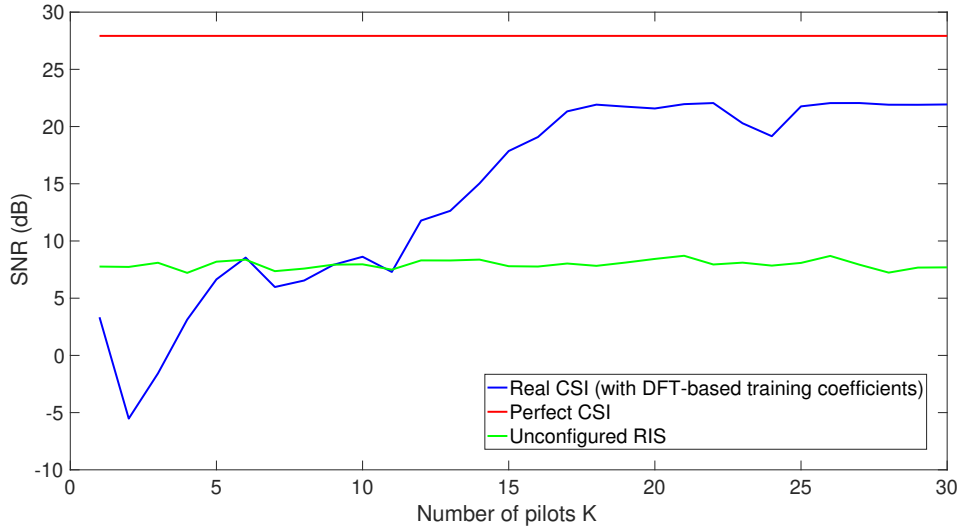

Figure 4.7: Results obtained exploiting the ML criterion (with 1000 iterations and setting the RIS with a random training pattern during the estimation phase of the channel). Simulations are made considering 100 Monte Carlo iterations, in order to mediate the noise effect.

the channel.
Extending our simulations, considering the transmitter located in the same position $(x = 0, y = 10, z = 1)$ and considering different points inside the room for the receiver, we are going to fix the following data:

- Number of pilot signals K equal to 30;
- Number of possible values of s equal to 1000;
- Number of Monte Carlo iterations equal to 100;

We obtain the following results:

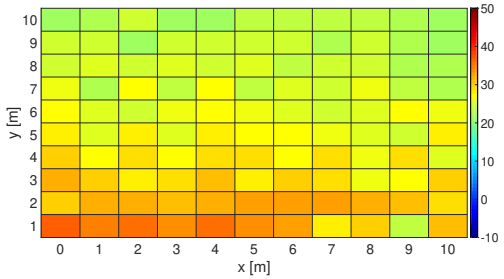

(a) SNR achievable at the receiver.

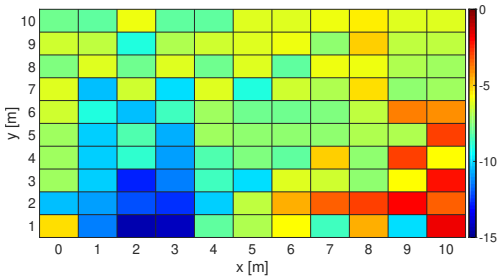

(b) Difference between the SNR obtained in the figure (a) and the best SNR achievable at the receiver with a perfect knowledge of CSI.

Figure 4.8: Heatmaps obtained with 30 pilot signals, based on the hypothesis of far-field.

In order to evaluate our approach, we need to compare it between the results obtained with an unconfigured RIS.

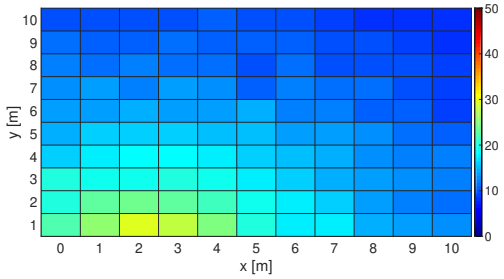

(a) SNR achievable at the receiver.

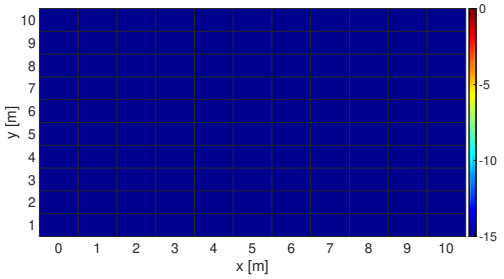

(b) Difference between the SNR obtained in the figure (a) and the best SNR achievable at the receiver with a perfect knowledge of CSI.

Figure 4.9: Heatmaps obtained with an unconfigured RIS.

As we can see comparing figures 4.8 and 4.9, results obtained with the ML research are much better than the ones obtained with an unconfigured RIS. Moreover, from figure 4.8 (b), it is interesting to note that:

1) The gap between the SNR obtained in the figure (a) and the best SNR achievable at the receiver with a perfect knowledge of CSI increase as we get closer to the RIS (because of the approximation of the EM as a plane wave fails);

2) Even in the most distance points from the RIS, the performance are not perfect (even though very good).

Near-field communication In order to overcome the limits imposed by the far-field hypothesis, we extend our simulation assuming a more accurate approximation of the wave front shape. In particular, we are going to simulate the ML criterion in the assumption of near-field communication. In this case, how previously said, we need to make a joint research about the terms $sin(\alpha) + sin(\beta)$ and dF. Keeping in mind that in far-field simulations we have exploited the research through 1000 different values of the gradient, now we need to consider a lower number in order to obtain results in a reasonable time. In particular, through different simulations, we have obtained good results in the previous scenario also considering 250 different values of the gradient. As the proof of this, heatmaps obtained are shown below:

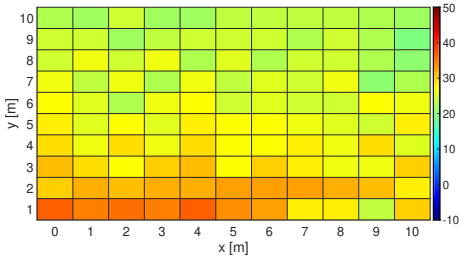

(a) SNR achievable at the receiver.

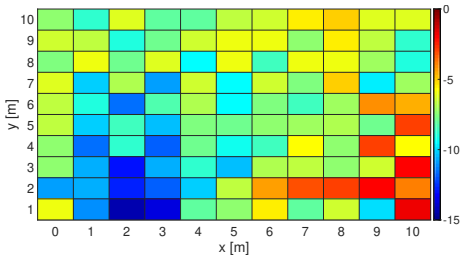

(b) Difference between the SNR obtained in the figure (a) and the best SNR achievable at the receiver with a perfect knowledge of CSI.

Figure 4.10: Heatmaps obtained with 30 pilot signals assuming 250 different values for s, instead of 1000) and under the hypothesis of far-field.

Comparing figures 4.8 and 4.10 the results are almost the same.

In order to choose a correct interval within which varying the value of the distance dF, it is important to recall that $\frac{1}{dF} = \frac{1}{dF_{TR}} + \frac{1}{dF_{RU}}$. Remembering

that dF_{TR} and dF_{RU} are respectively the distance between the transmitter and the center of the RIS and the distance between the center of the RIS and the receiver, dF will assume an increasingly larger value as the transmitter and receiver move away from the RIS and, vice versa, a lower value when transmitter and receiver come closer to it: so, the maximum value that we are expecting for dF will be equal to 5.6 meters (that corresponds to the case of transmitter and receiver as far as possible to the RIS). In our simulations it makes sense to consider $dF \in [0, 6]$ meters. Because of previously considerations, we are going to set up the following data for simulations:

- Number of pilot signals $K = 30$;
- Number of different values for the term referring to $sin(\alpha) + sin(\beta)$ equal to 250 (chosen in the interval [-1,1], as previously explained);
- Number of different values for the term referring to dF equal to 100;
- Number of Monte Carlo iterations equal to 10.

Fixing the transmitter in $(x = 0, y = 10, z = 1)$ and varying the positions of the receiver, we obtain the following results:

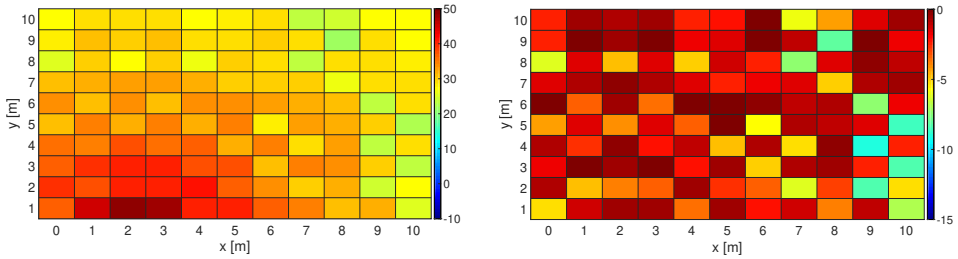

(a) SNR achievable at the receiver

(b) Difference between the SNR obtained in the figure (a) and the best SNR achievable at the receiver with a perfect knowledge of CSI.

Figure 4.11: Heatmaps obtained with 30 pilot signals, based on the hypothesis of near-field.

As we can see, considering a more detailed approximation of the EM field impinging to the RIS brings to better performance, especially where the transmitter or the receiver (or both) are near to the RIS.

4.4 Trade-off between SNR and number of pilot signals

Keeping in mind the obtained results, the proposed method allows us to reach good performance exploiting much less pilot signals rather than that requested in the optimal method. In particular, the best performance of our approach is reached with the 30% of the number N of elements of the RIS. Rearranging the data extrapolated from the figure 4.6, that it refers to the case of transmitter at $(x = 0, y = 10, z = 10)$ and receiver at $(x = 10, y = 10, z = 1)$, we can better visualize the difference of the performance obtained between the proposed method and the best achievable results obtainable only with a perfect estimation of CSI:

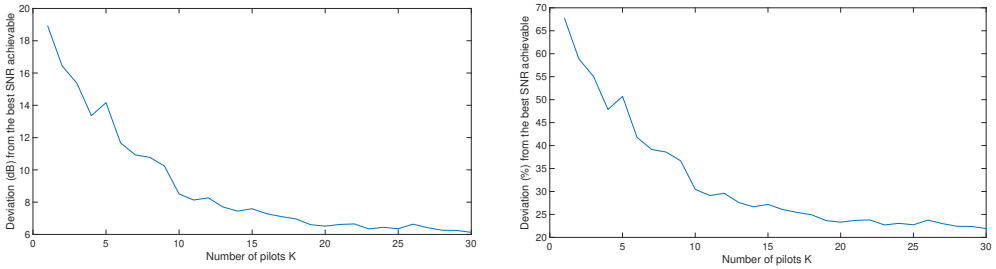

(a) Difference between performance with perfect and imperfect CSI, in function of the number of pilot signals.

(b) Difference (%) between performance with perfect and imperfect CSI, as a function of the number of pilot signals.

Figure 4.12: Deviation from the best SNR achievable.

As we can see from figure 4.12, it exists a saturation curve which begins approximately at 10% of the pilot signals.
Because of our goal is to reduce the overhead training as much as possible (without degrading "too much" the performance), we can consider a trade-off between the number of pilot signals and the performance desired. For example, if we are willing to accept a SNR lower than the 10-15% of the maximum possible value, we can exploit less pilot signals. As we can see in figure 4.13, always in those particular positions of transmitter and receiver, accepting a performance degraded of 10% lower then the best achievable, permits to reduce the number of the training signals at 12-13% of the ones needed in the method proposed in Chapter 3.

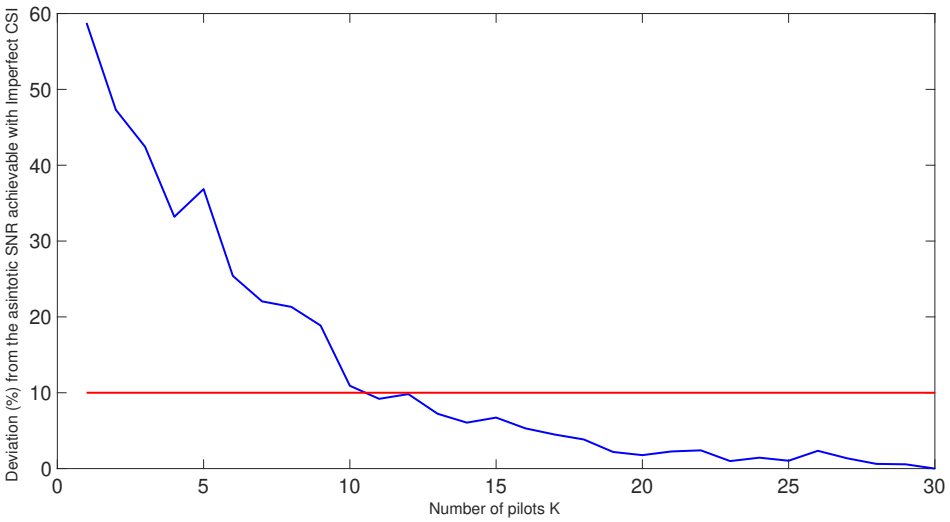

Figure 4.13: Difference (%) between performance obtained, in function of the number of pilot signals, in comparison to the best achievable obtainable with 30% of signals.

4.5 Extension of the method for a planar RIS

In the previous analysis, we have considered a stripe RIS. In this section, we are going to show the cascaded channel expression in presence of a planar RIS, both for far-field and near-field communication. In particular, we are going to consider a planar RIS arranged on the same wall as the previous scenario, on the XZ-plane.

4.5.1 Far-field communication

Keeping in mind that a planar RIS is arranged on the XZ-plane, while transmitter and receiver are placed at the height of $z = 1$ meter and can be placed in generic points inside the room on the plane (x, y), we have to note that the phase gradients of the channels $\mathbf{h_{TR}}$ and $\mathbf{h_{RU}}$ are both bi-dimensional. Because of we can represent a planar RIS as a matrix of N reflecting elements, the expressions of the two channels becomes:

$$h_{TR_{n,m}} = q_1 \cdot e^{i\frac{2\pi}{\lambda}\cdot\Delta\cdot(n-1)\cdot sin(\alpha_1)+i\frac{2\pi}{\lambda}\cdot\Delta\cdot(m-1)\cdot sin(\alpha_2)}, \tag{4.8}$$

$$h_{RU_{n,m}} = q_2 \cdot e^{i\frac{2\pi}{\lambda}\cdot\Delta\cdot(n-1)\cdot sin(\beta_1)+i\frac{2\pi}{\lambda}\cdot\Delta\cdot(m-1)\cdot sin(\beta_2)}, \tag{4.9}$$

$\forall n = 1, \dots A, \quad \forall m = 1, \dots B$, where A and B represents respectively the number of reflecting elements for every row and for every column of the

planar RIS. Moreover, α_1 and α_2 represent respectively the horizontal angles of incidence between the EM field and RIS and the vertical one. The same is for β_1 and β_2 referring to the channel between RIS and receier.
In far-field communications, referring to the channel between transmitter and RIS, the terms $sin(\alpha_1)$ and $sin(\alpha_2)$ remains constants for every element of the RIS. The same is for the terms $sin(\beta_1)$ and $sin(\beta_2)$, referred to the channel between the RIS and the receiver. The cascaded channel vector will be:

$$h_{n,m} = k \cdot e^{i\frac{2\pi}{\lambda}\cdot\Delta\cdot\left((n-1)\cdot(sin(\alpha_1)+sin(\beta_1))+(m-1)\cdot(sin(\alpha_2)+sin(\beta_2))\right)} \tag{4.10}$$

$\forall n = 1, \dots A, \quad \forall m = 1, \dots B$. Recalling d_1 as $sin(\alpha_1) + sin(\beta_1)$ and d_2 as $sin(\alpha_2) + sin(\beta_2)$, the ML criterion consist on the jointly research of these two parameters.

4.5.2 Near-field communication

In near-field communication, in analogy to the case of stripe RIS, we have to consider also the term referred to the focal distance. The expression (4.11) will become:

$$h_{n,m} = k \cdot e^{i\frac{2\pi}{\lambda}\cdot\left(\Delta\left((n-1)\cdot d_1+(m-1)\cdot d_2\right)+\frac{\left((\Delta(n-1))^2+(\Delta(m-1))^2\right)}{2\cdot dF}\right)} \tag{4.11}$$

$\forall n = 1, \dots A, \quad \forall m = 1, \dots B$. In this case, the ML criterion consists on the jointly research of three terms:

- d_1
- d_2
- dF

where dF we remember is the total contribute of the focal distance of the channel between transmitter and RIS and the channel between RIS an receiver.

4.6 Relation between CSI and user position

In a free-space scenario, as the one we treated until now, the CSI is strongly related to the position of the transmitter, receiver and RIS. In fact, in a free-space scenario, fixed the transmitter and the RIS positions, a particular

phase profile of the cascaded channel $\mathbf{h}$ is associated to any user position. According to this, the CSI estimation can be useful also to localize the user position.
Anyway, without knowing the coordinates of the transmitter and the RIS, it is not possible to trace back from the cascaded channel to the user position because a generic phase profile of $\mathbf{h}$ is obtained by the combined effect of the channels $\mathbf{h_{TR}}$ and $\mathbf{h_{RU}}$. Because of the CSI is related to the positions of the transmitter, receiver and RIS, this is perfectly in line as previously said: as without the knowledge of the transmitter and the RIS positions we can not get an estimate of the channels $\mathbf{h_{TR}}$ and $\mathbf{h_{RU}}$, but only their cascaded $\mathbf{h}$, at the same way it is not possible to trace back to the transmitter/receiver position from the knowledge of the cascaded channel.

4.6.1 A method to estimate the user position

In the hypothesis to know the transmitter and RIS positions, and after estimating the cascaded channel (for example, with the ML criterion), it is possible to estimate the user position making a comparison between $\hat{\mathbf{h}}$ and all the possible cascaded channel vectors associated to all the possible positions of the receiver. In particular, knowing the position of the transmitter and the RIS, it is possible to calculate the cascaded channel vector for any user position and collect the results into a look-up table. So, fixed a number P of the total possible different positions of the user taking into account, a loop-up table is created saving the P vectors calculated.
In reality, it is possible to estimate the position of the receiver even without estimating the channel directly: it is sufficient to save in the loop-up table the global channel effect g for every user position and compare them with (theoretically) a single collected measure $\hat{g}$ made by the receiver.
In order to evaluate this approach, we are going to consider and simulate the same scenario described until now, considering the position of the user variable inside the room.
In order to create the loop-up table, we need to select a grid representing the possible positions for the receiver, taking into account that a grid too large slows down the calculation times. In our simulations, we divide the room into a grid with a step equal to 10 cm, remembering that this is also the maximum resolution that we can have. So, after choosing the number K of pilot tones to send and the RIS configurations, we can collect K measurements of g, saved in a vector $\hat{\mathbf{g}}$, in order to compare them with the values saved in the loop-up table.
We can schematize the algorithm as follows:

1. Select the number P of the cascaded channels to save in the look up-table;

2. Select the number K of pilot signals;

3. Select K different configuration of the RIS, one for every pilot signal (it can be the same also);

4. Create a look-up table $\mathbf{G}$ of dimension $P \times N$, where the generic ith row represents the cascaded channel vector related the ith position of the receiver;

5. The receiver collects K noisy measurements of g, represented in the vector $\hat{\mathbf{g}}$;

6. The receiver calculates the norm of the difference between every row of $\mathbf{G}$ and $\hat{\mathbf{g}}$;

7. The receiver estimates its coordinates selecting those that refer to the position that gave rise to the least difference.

4.6.2 Position maximum likelihood estimator

In order to simulate this approach in the same scenario, we consider:

- A grid with a step equal to 10 cm;
- $K = 30$;
- A random configuration of the RIS (that it remains the same for every pilot signal);

Repeating the algorithm for 1000 random positions of the user inside the room, and considering 100 Monte Carlo iterations for every problem in order to mediate the noise effect, we obtain the following result shown in figure 4.14, which shows the empirical cumulative distribution function (CDF) of the root mean square error (RMSE) of the position estimation. As we can see, a RIS with more elements allows to better estimate the position of the receiver. This result is in agreement with the fact that having more elements is equivalent to having an increasingly unique phase profile that permits to be more robust on noise.
Since the estimation error also depends on how fine the grid of positions is, we can repeat the same simulation considering a new grid with a step equal to 20 cm. The results are shown in figure 4.15.

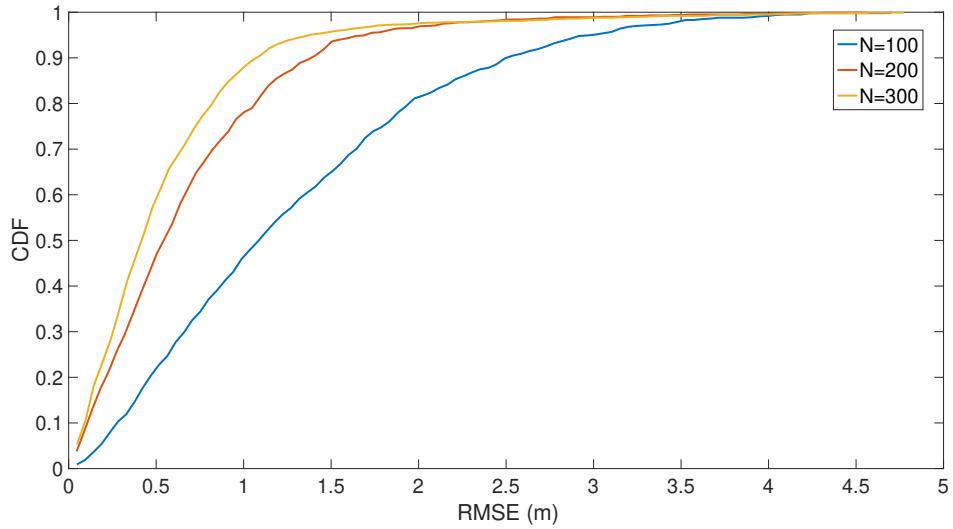

Figure 4.14: CDF of the position estimation RMSE considering 1000 random positions of the user, a grid with step equal to 10 cm and a RIS composed by N reflecting elements.

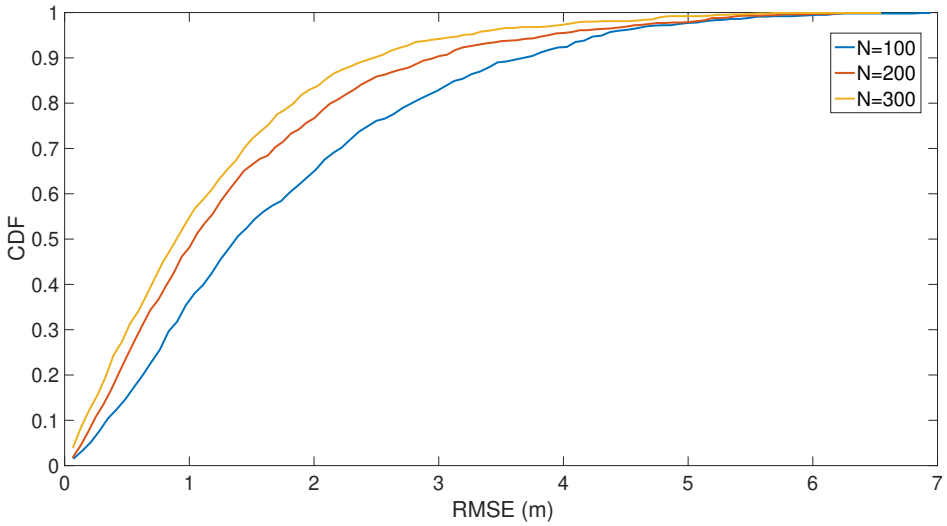

Figure 4.15: CDF of the position estimation RMSE considering 1000 random positions of the user, a grid with step equal to 20 cm and a RIS composed by N reflecting elements.

Making a comparison between the results in figure 4.14 and 4.15, we can plot them together (figure 4.16).

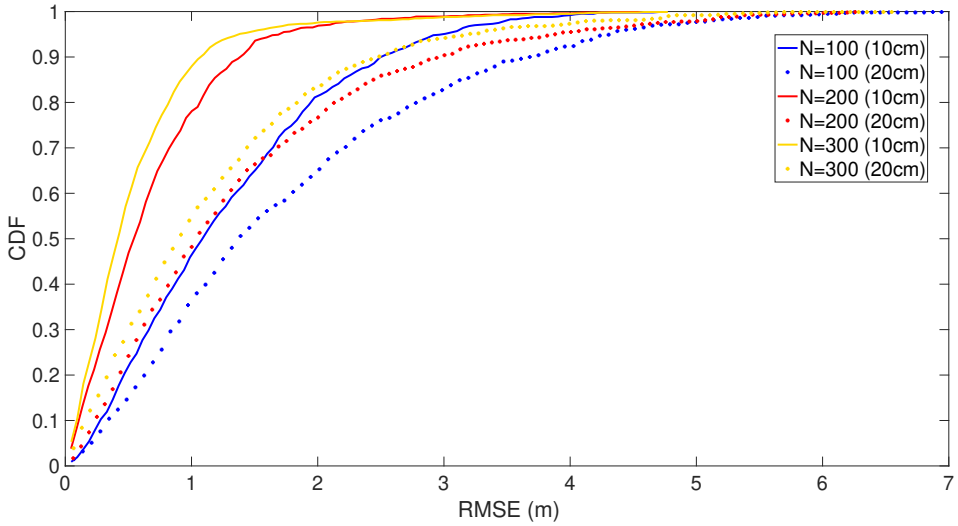

Figure 4.16: Comparison between CDF of the position estimation RMSE considering 1000 random positions of the user and a grid with step equal to 10 cm and 20 cm.

The results obtained indicate with that large RIS it is possible to localize with sub-meter accuracy in more than 90% of locations without the need of deploying more base stations as required in the conventional positioning system. In order to see what happens with a grid with few positions, we repeat the simulation considering a step equal to 1 meter. The results are shown in figure 4.17. As we can see, this approach for the estimation of the user position is valid only with sufficient fine grids.

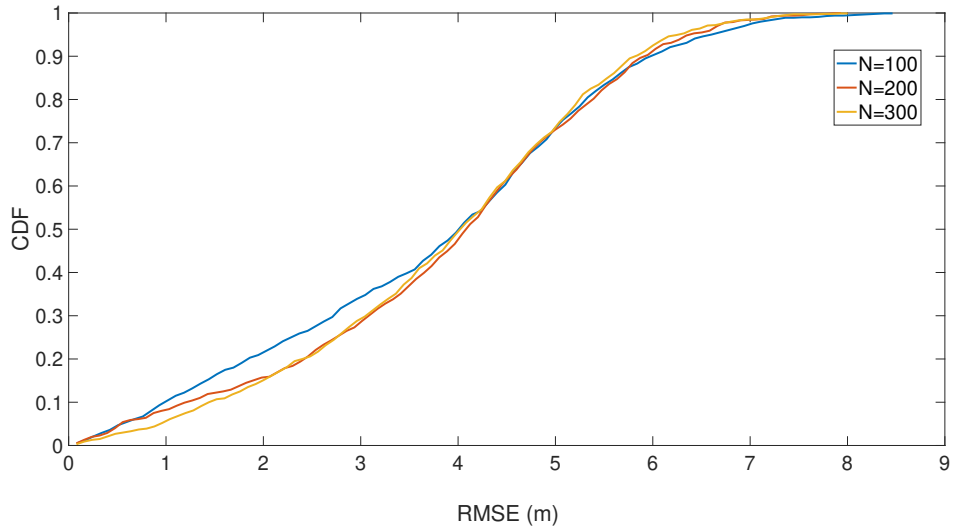

Figure 4.17: CDF of the position estimation RMSE considering 1000 random position of the user and a grid with step equal to 1 meter.

Chapter 5

Conclusions and perspective

The thesis activity developed is about the study of RIS-assisted wireless networks. One of the main problems of these networks has always concerned the estimation of the CSI due to the high number of pilot tones required, even in the simplest SISO systems. After having analyzed the main approaches present in literature regarding the channel estimation, we have presented a novel algorithm, based on the ML criterion, able to estimate the CSI with a reduced number of pilot tones. In fact, how shown in our simulations, the approach proposed allows to obtain a good estimate of the channel with only 10/15% of the pilot tones required by the main optimal approaches studied. Furthermore, considering that the channel estimation problem is strictly related to the user position, it was also possible to adapt the algorithm to estimate the position of the receiver without the need of any anchor node (as it is necessary in current real-time location system). The idea of adopting a RIS to assist the communication in order to improve the SNR at the receiver is probably the future of the next communication systems based on frequencies of the order of terahertz, as it represents a simple and economical solutions, which does not require additional hardware and which reduce wasting power.
It can be interesting to extend our channel estimation approach also for the MIMO case and to think of a strategy applicable for multiple users and/or multiple RIS.

List of Figures

Bibliography

[1] Qingqing Wu and Rui Zhang: *Towards Smart and Reconfigurable Environment: Intelligent Reflecting Surface Aided Wireless Network*, in IEEE Communications Magazine, vol. 58, no. 1, pp. 106-112, January 2020, doi: 10.1109/MCOM.001.1900107.

[2] Walid Saad, Mehdi Bennis, and Mingzhe Chen: *A Vision of 6G Wireless Systems: Applications, Trends, Technologies, and Open Research Problems*, in IEEE Network, vol. 34, no. 3, pp. 134-142, May/June 2020, doi: 10.1109/MNET.001.1900287.

[3] Hadi Sarieddeen, Nasir Saeed, Tareq Y. Al-Naffouri, and Mohamed-Slim Alouini: *Next Generation Terahertz Communications: A Rendezvous of Sensing, Imaging and Localization*, in IEEE Communications Magazine, vol. 58, no. 5, pp. 69-75, May 2020, doi: 10.1109/MCOM.001.1900698.

[4] Marco Di Renzo, Alessio Zappone, Merouane Debbah, Mohamed-Slim Alouini, Chau Yuen, Julien de Rosny, and Sergei Tretyakov: *Smart Radio Environments Empowered by Reconfigurable Intelligent Surfaces: How it Works, State of Research, and Road Ahead*, in IEEE Journal on Selected Areas in Communications, vol. 38, no. 11, pp. 2450-2525, Nov. 2020, doi: 10.1109/JSAC.2020.3007211.

[5] Sha Hu, Fredrik Rusek and Ove Edfors: *Beyond Massive MIMO: The Potential of Positioning With Large Intelligent Surfaces*, in IEEE Transactions on Signal Processing, vol. 66, no. 7, pp. 1761-1774, 1 April1, 2018, doi: 10.1109/TSP.2018.2795547.

[6] Marco Di Renzo, Merouane Debbah, Dinh-Thuy Phan-Huy, Alessio Zappone, Mohamed-Slim Alouini, Chau Yuen, Vincenzo Sciancalepore, George C. Alexandropoulos, Jakob Hoydis, Haris Gacanin, Julien de Rosny, Ahcene Bounceur, Geoffroy Lerosey and Mathias Fink: *Smart radio environments empowered by reconfigurable AI meta-surfaces: an*

idea whose time has come, J Wireless Com Network 2019, 129 (2019). https://doi.org/10.1186/s13638-019-1438-9

[7] Qingqing Wu, Shuowen Zhang, Beixiong Zheng, Changsheng You, and Rui Zhang: *Intelligent Reflecting Surface Aided Wireless Communications: A Tutorial*, arXiv:2007.02759 [cs.IT] (2020)

[8] Mohamed A. ElMossallamy, Hongliang Zhang, Lingyang Song, Karim G. Seddik, Zhu Han, and Geoffrey Ye Li: *Reconfigurable Intelligent Surfaces for Wireless Communications: Principles, Challenges, and Opportunities*, arXiv:2005.00938 [eess.SP] (2020)

[9] Marco di Renzo: *6Gwireless: Wireless Networks Empowered by Reconfigurable Intelligent Surfaces*, Nokia Bell Labs - Blanchardstown Business and Technology Park - September 5, 2019 - Dublin, Ireland

[10] Christos Liaskos, Shuai Nie, Ageliki Tsioliaridou, Andreas Pitsillides, Sotiris Ioannidis, and Ian Akyildiz: *A New Wireless Communication Paradigm through Software-Controlled Metasurfaces*, in IEEE Communications Magazine, vol. 56, no. 9, pp. 162-169, Sept. 2018, doi: 10.1109/MCOM.2018.1700659.

[11] Samith Abeywickrama, Rui Zhang, Qingqing Wu, and Chau Yuen: *Intelligent Reflecting Surface: Practical Phase Shift Model and Beamforming Optimization*, arXiv:1907.06002 [eess.SP] (2020)

[12] George C. Alexandropoulos and Evangelos Vlachos: *A Hardware Architecture for Reconfigurable Intelligent Surfaces with Minimal Active Elements for Explicit Channel Estimation*, arXiv:2002.10371 [cs.IT] (2020)

[13] Abdelrahman Taha, Muhammad Alrabeiah, and Ahmed Alkhateeb: *Enabling Large Intelligent Surfaces with Compressive Sensing and Deep Learning*, arXiv:1904.10136 [cs.IT] (2019)

[14] Abdelrahman Taha, Muhammad Alrabeiah, and Ahmed Alkhateeb: *Deep Learning for Large Intelligent Surfaces in Millimeter Wave and Massive MIMO Systems*, 2019 IEEE Global Communications Conference (GLOBECOM), Waikoloa, HI, USA, 2019, pp. 1-6, doi: 10.1109/GLOBECOM38437.2019.9013256.

[15] Abdelrahman Taha, Yu Zhang, Faris B. Mismar, and Ahmed Alkhateeb: *Deep Reinforcement Learning for Intelligent Reflecting Surfaces: Towards Standalone Operation*, arXiv:2002.11101 [cs.IT] (2020)

[16] Weifeng Han, Peng Chen, and Zhenxin Cao: *Deep Neural Network-Based Quantized Signal Reconstruction for DOA Estimation*, arXiv:2005.01102 [eess.SP] (2020)

[17] Deepak Mishra and Hakan Johansson: *Channel Estimation and Low-Complexity Beamforming Design for Passive Intelligent Surface Assisted MISO Wireless Energy Transfer*, ICASSP 2019 - 2019 IEEE International Conference on Acoustics, Speech and Signal Processing (ICASSP), Brighton, UK, 2019, pp. 4659-4663, doi: 10.1109/ICASSP.2019.8683663.

[18] Changsheng You, Beixiong Zheng, and Rui Zhang: *Intelligent Reflecting Surface with Discrete Phase Shifts: Channel Estimation and Passive Beamforming*, arXiv:1911.03916 [cs.IT] (2019)

[19] Peilan Wang, Jun Fang, Huiping Duan, and Hongbin Li: *Compressed Channel Estimation for Intelligent Reflecting Surface-Assisted Millimeter Wave Systems*, in IEEE Signal Processing Letters, vol. 27, pp. 905-909, 2020, doi: 10.1109/LSP.2020.2998357.

[20] Zhen-Qing He and Xiaojun Yuan: *Cascaded Channel Estimation for Large Intelligent Metasurface Assisted Massive MIMO*, arXiv:1905.07948 [cs.IT] (2020)

[21] Gilderlan T. de Araujo, and Andrè L. F. de Almeida: *PARAFAC-Based Channel Estimation for Intelligent Reflective Surface Assisted MIMO System*, arXiv:2001.06554 [eess.SP](2020)

[22] Jawad Mirza, and Bakhtiar Ali: *Channel Estimation Method and Phase Shift Design for Reconfigurable Intelligent Surface Assisted MIMO Networks*, arXiv:1912.10671 [cs.IT] (2020)

[23] Jiguang He, Markus Leinonen, Henk Wymeersch, and Markku Juntti: *Channel Estimation for RIS-Aided mmWave MIMO Channels*, arXiv:2002.06453 [eess.SP] (2020)

[24] Saud Khan, Komal S Khan, Noman Haider, and Soo Young Shin: *Deep-Learning-Aided Detection for Reconfigurable Intelligent Surfaces*, arXiv:1910.09136 [eess.SP] (2020)

[25] Ahmet M. Elbir, Anastasios Papazafeiropoulos, Pandelis Kourtessis, and Symeon Chatzinotas: *Deep Channel Learning For Large Intelligent Surfaces Aided mm-Wave Massive MIMO Systems*, arXiv:2001.11085 [eess.SP] (2020)

[26] Boyu Ning, Zhi Chen, Wenrong Chen, and Yiming Du: *Channel Estimation and Transmission for Intelligent Reflecting Surface Assisted THz Communications*, arXiv:1911.04719 [cs.IT] (2020)

[27] Boyu Ning, Zhi Chen, Wenrong Chen, Yiming Du, and Jun Fang: *Terahertz Multi-User Massive MIMO with Intelligent Reflecting Surface: Beam Training and Hybrid Beamforming*, arXiv:1912.11662 [cs.IT] (2021)

[28] Beixiong Zheng, Changsheng You, and Rui Zhang: *Uplink Channel Estimation for Double-IRS Assisted Multi-User MIMO*, arXiv:2010.06155 [cs.IT] (2020)

[29] Davide Dardari, and Devis Massari: *Using MetaPrisms for Performance Improvement in Wireless Communications*, arXiv:2003.13505 [eess.SP] (2020)

[30] Ahmed Elzanaty, Anna Guerra, Francesco Guidi, and Mohamed-Slim Alouini: *Reconfigurable Intelligent Surfaces for Localization: Position and Orientation Error Bounds*, arXiv e-prints, p. arXiv:2009:02818, Sep. 2020.

[31] Davide Dardari: *Communications with Large Intelligent Surfaces: Fundamental Limits and Models*, in IEEE Journal on Selected Areas in Communications, vol. 38, no. 11, pp. 2526-2537, Nov. 2020, doi: 10.1109/JSAC.2020.3007036.